Kansas Geological Survey

Approximate Analysis of Groundwater Mineralization Due to Local Discontinuity in an Impermeable Layer
Part 1: Direct Contact between Fresh and Saltwater

By

Hillel Rubin* and Robert W. Buddemeier
Kansas Geological Survey, The University of Kansas
Lawrence, KS 66047

Kansas Geological Survey Open File Report 98-31
July 24, 1998

GEOHYDROLOGY

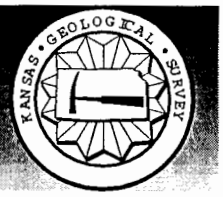

The University of Kansas, Lawrence, KS 66047 Tel. (785) 864-3965

Kansas Geological Survey
Open-file Report

Disclaimer

The Kansas Geological Survey does not guarantee this document to be free from errors or inaccuracies and disclaims any responsibility or liability for interpretations based on data used in the production of this document or decisions based thereon. This report is intended to make results of research available at the earliest possible date, but is not intended to constitute final or formal publication.

Approximate Analysis of Groundwater Mineralization Due to Local Discontinuity in an Impermeable Layer
Part 1: Direct Contact between Fresh and Saltwater

Hillel Rubin* and Robert W. Buddemeier
Kansas Geological Survey, The University of Kansas
Lawrence, KS 66047

Abstract

This manuscript represents a basic study carried out within a framework of comprehensive research on the major mechanisms and phenomena involved in the mineralization of groundwater of the Great Bend Prairie aquifer in Kansas by saltwater originating from a deeper Permian bedrock formation. The conceptual model for this study assumes that mineralization of the aquifer is attributed to local discontinuities in the impermeable layers, which allow direct contact between the fresh and saline water.

Calculations are made for a single discontinuity in the impermeable layer. Salinity penetrating into the freshwater aquifer through that discontinuity is subject to advection and dispersion. A boundary layer (BL) method developed in the framework of this study provides a simple but robust approach for the initial evaluation of mineralization processes taking place downstream of the local discontinuity in the impermeable layer. It was shown that downstream of the discontinuity, the salinity profiles incorporate two BLs: an inner BL adjacent to the bottom of the aquifer, and an outer BL, which develops on top of the inner one. The horizontal penetration of the salinity is characterized by two regions extending along the aquifer: the steady state region and the spearhead region. The latter represents the salinity front, which varies as a function of the discontinuity exposure length, distance from the discontinuity, and the aquifer characteristics.

---

* On leave from the Department of Civil Engineering, Technion—Israel Institute of Technology, Haifa 32000, Israel.

The method developed in this study has been applied to practical issues concerning mineralization of groundwater in south central Kansas.

Introduction

This manuscript addresses the interest in understanding major mechanisms and phenomena involved in the mineralization of the Great Bend Prairie aquifer of south central Kansas. The Great Bend Prairie aquifer overlies bedrock of Cretaceous and Permian age. Various publications provide information concerning the geology of the region (e.g. Latta, 1950; Layton and Berry, 1973; Fader and Stullken, 1978; Cobb, 1980). During the last few years significant efforts have been invested in measuring salinity distribution in the region (Young, 1992; Whittemore, 1993; Buddemeier et al. 1992; 1994; Garneau, 1995; Quinodoz and Buddemeier, 1997; Young and Rubin, 1998). These measurements were analyzed and used for the identification of sources of salinity, as well as mechanisms involved in the mineralization processes.

Rubin and Buddemeier(1996; 1998a;b) have developed conceptual and modeling approaches known as the top specified boundary layer (TSBL) method. Two previous articles have applied the TSBL method to the analysis of direct contact between fresh and saline groundwater (Rubin and Buddemeier, 1998a) and to seepage through a semi-confining layer separating the fresh and saline portions of the aquifer (Rubin and Buddemeier, 1998b). Both of these previous studies addressed an interface that was unlimited in its horizontal dimensions (i.e., on the order of km or larger). These approaches have been applied to evaluation of salinity profiles and to obtaining characteristic values of dispersivity (Garneau, 1995). Some studies have also applied the TSBL method in conjunction with measurements of pressures in various depths (Young and Rubin, 1998) and calculations of salt budget in various sections of the aquifer (Quinodoz and Buddemeier, 1997).

In most places clay and shale layers effectively separate the freshwater aquifer from the saline water of the deep formations. Salinity penetrations are probably local phenomena, occurring through the discontinuities in the impermeable layer in spatially limited locations. However, once it penetrates into the freshwater aquifer, the salinity is advected, disperses and thereby contaminates the freshwater resources of the region. In this report (Part 1 of the present

study) we consider salinity penetration into the freshwater aquifer due to direct contact between the freshwater and the deeper saline water at discontinuities in an impermeable confining layer which have dimensions smaller than or comparable to the vertical dimensions of the aquifer (i.e., a magnitude on the order of 100 m or less). Saline water may also penetrate into the freshwater aquifer due to infiltration through semipermeable discontinuities in the confining layer; this phenomenon is considered in the following report (part 2 of the present study).

The Conceptual Model and Basic Formulation

The simplified conceptual model is shown in Fig. 1. This model describes a local discontinuity in an impermeable layer that separates saline and fresh water aquifers that are otherwise identical. This discontinuity causes direct contact between fresh and saline water along the exposure length, x_e^*.

Flow conditions and salinity transport in the complete domain of Fig. 1 are governed by the following set of differential equations:

$$\vec{q} = -\frac{k}{\mu}(\nabla p - \rho \vec{g}) \tag{1}$$

$$\frac{\partial C^*}{\partial t^*} + \vec{V} \cdot \nabla C^* = \nabla \cdot \left(\tilde{D} \cdot \nabla C^*\right) \tag{2}$$

where $\vec{q}$ is the specific discharge vector, k is the permeability; μ is the fluid viscosity; p is the pressure; ρ is the fluid density; g is the gravitational acceleration; C^* is the salt concentration (salinity); $\vec{V}$ is the vector of interstitial flow velocity; $\tilde{D}$ is the dispersion tensor; t^* is time.

Equations (1) and (2) represent a set of differential equations, which can be solved by various types of numerical procedures. However, the simultaneous solution of eqs. (1) and (2) is quite complicated; the non linearity stemming from the dependence of ρ on C^* introduces simulation difficulties, and there are problems of stability of the numerical solution, numerical dispersion, etc. Therefore, an introduction of some simplifications into the calculation of salinity

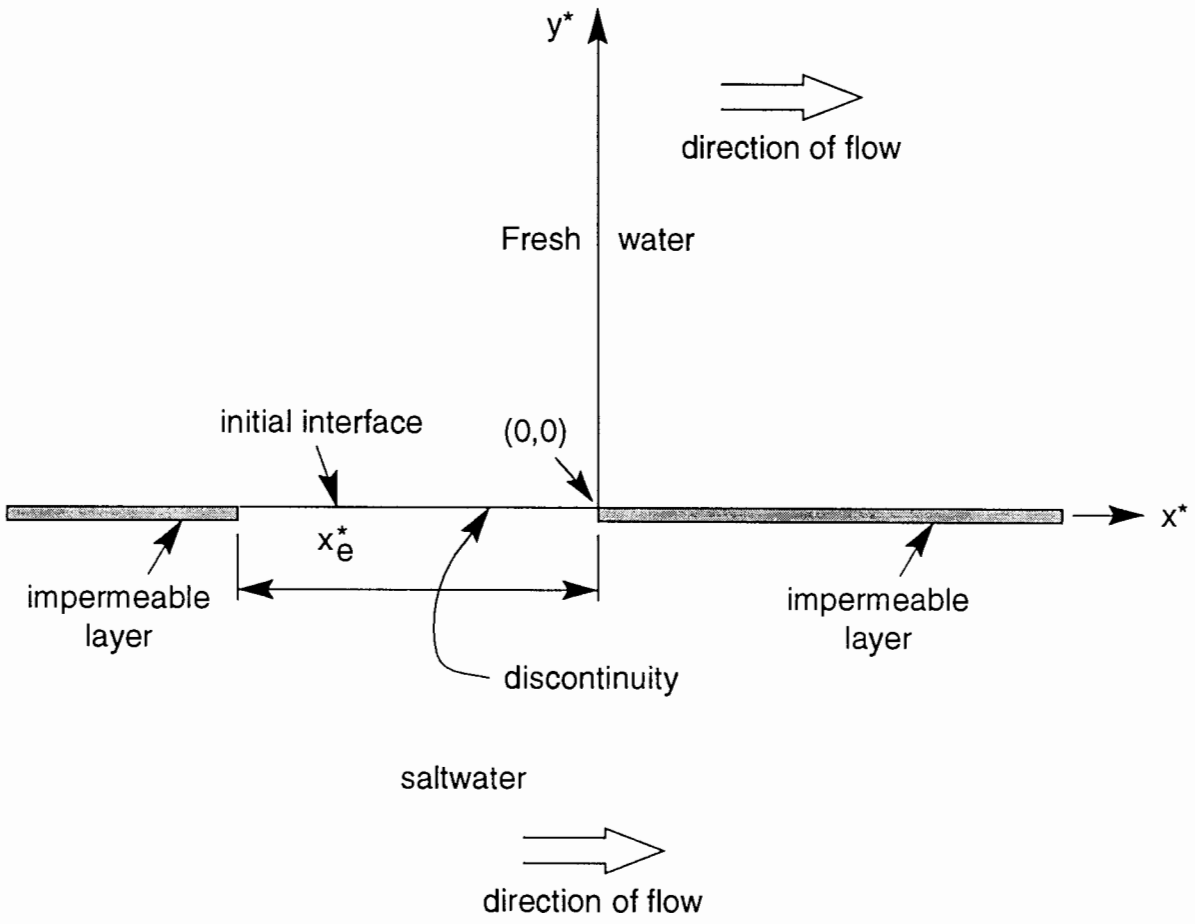

Fig. 1. Conceptual model of an aquifer subject to salinity penetration through a local discontinuity in an impermeable layer.

transport in the domain of Fig. 1 is very desirable. Such simplification should be consistent with a methodology of groundwater quality simulation in stages. The initial stage of such a methodology consists of general quantitative evaluation of phenomena and the time scales of contamination and reclamation, as well as initial risk analysis. This paper addresses such a limited stage. Some possible simplifications introduced into eqs. (1) and (2) for the initial stage of groundwater quality calculation in the domain of Fig. 1 are given in the following paragraphs.

Initially, the upper part of the domain, represented by $y^* \geq 0$, is occupied by freshwater, and a sharp interface between the fresh and saline water exists at the discontinuity exposure length, x_e^*; namely at

$$y^* = 0, \qquad -x_e^* \leq x^* \leq 0 \tag{3}$$

The density and total dissolved solids (TDS) of the saltwater present in the Permian zone are very similar to those of seawater (Whittemore, 1993). Therefore, effects of salinity on the groundwater viscosity are minor, and thereby the hydraulic conductivity of the domain shown in Fig. 1 may be considered almost uniform. We may also employ the Dupuit approximation and consider that streamlines are horizontal. Then eq. (1) indicates that the velocity V is uniformly distributed in the domain, and it has only a component in the x^* direction. Therefore, salinity transport in the domain is governed by

$$\frac{\partial C^*}{\partial t^*} + V\frac{\partial C^*}{\partial x^*} = D_x \frac{\partial^2 C^*}{\partial x^{*2}} + D_y \frac{\partial^2 C^*}{\partial y^{*2}} \tag{4}$$

where x^* and y^* are the longitudinal and vertical coordinates, respectively; D_x and D_y are the longitudinal and transverse dispersion coefficients, respectively.

The assumed uniformity of the physical parameters in the domain of Fig. 1 causes a complete asymmetry of the salinity distribution in that domain. It is also possible to apply dimensionless quantities instead of the physical coordinates and variables, defined by

$$x = x^* / l_0;\ y = y^* / l_0;\ t = t^* V / l_0$$
$$C = \left(C^* - C_f^*\right) / \left(C_s^* - C_f^*\right) \tag{5}$$

where l_0 is an adopted unit length along the initial interface; C_s^* is the salinity of the saltwater, and C_f^* is the salinity of the freshwater.

Introducing the dimensionless variables of eq. (5) into eq. (4) we obtain

$$\frac{\partial C}{\partial t} + \frac{\partial C}{\partial x} = a_L \frac{\partial^2 C}{\partial x^2} + a \frac{\partial^2 C}{\partial y^2} \tag{6}$$

where aL and a are the dimensionless longitudinal and transverse dispersivities, which are defined by

$$a_L = D_x / \left(l_0 V\right); \qquad a = D_y / \left(l_0 V\right) \tag{7}$$

The mineralization process in the region

$$y \geq 0; \qquad -x_e \leq x \leq 0 \tag{8}$$

where $x_e = x_e^* / l_0$, has been analyzed by Rubin and Buddemeier (1998a). The present study employs results obtained in that study, and concentrates of efforts on simulating the salinity transport in the region

$$x, y \geq 0 \tag{9}$$

The study of Rubin and Buddemeier (1998a) indicates that the initial interface at the discontinuity of the impermeable layer represents the isohaline C = 0.5. On both sides of that isohaline a transition zone (TZ) develops. The transition zone that develops in the domain part given by eq. (9) is called the region of interest (ROI) in which salinity exceeds the acceptable value. Applying the results of Rubin and Buddemeier (1998a) we inferred that in the region specified by eq. (8) steady state conditions are obtained at $t = x_e$. During the time interval

$$0 \leq t \leq x_e \tag{10}$$

a salinity profile develops at the downstream edge of the discontinuity, namely at

$$0 \le y \le \infty, \qquad x = 0 \tag{11}$$

Referring to eq. (6), it is possible to ignore the first right-hand side term of eq. (6) and obtain the following expression for the steady state salinity distribution at the downstream edge of the discontinuity, which is represented by eq. (11).

$$C = 0.5\ erfc\left(\frac{y}{2\sqrt{ax_e}}\right) \tag{12}$$

where *erfc* is the complementary error function.

The expression given by eq. (12) could be applied to the simulation of steady state salinity distribution in the domain specified by eq. (9), provided that the longitudinal extent of the domain was limited ($x \le x_{max}$), and steady state conditions were established. However, by applying the top specified boundary layer (TSBL) approach, Rubin and Buddemeier (1998a) concluded that at the boundary of eq. (11) the salinity distribution is

$$C = 0.5\left(1 - y / \delta_0\right)^n \tag{13}$$

$$\left(\delta_0^2\right)_{x=0} = 2an(n+1)\left[t - (t - x_e)u(t - x_e)\right] \tag{14}$$

where

$$u(t - x_e) = \begin{cases} 1 & t > x_e \\ 0 & t < x_e \end{cases} \tag{15}$$

The parameter δ_0 represents the value of y at which the salinity is smaller by at least an order of magnitude than some acceptable value. For the purpose of this derivation, the acceptable value of salinity defining the top of the ROI was considered to be $C_T = 0.005$, namely one percent of the salinity at the initial interface. For a wide range of values of the transverse dispersivity Rubin and Buddemeier (1998a) showed that the power coefficient of eq. (13) should be $n = 3$.

In the domain of eq. (9) the salinity distribution should be determined by the boundary condition of eq. (12) or (13) as well as by the boundary conditions

$$\frac{\partial C}{\partial y} = 0 \quad at \quad y = 0$$
$$C \to 0 \quad at \quad y \to \infty \tag{16}$$
$$C = 0 \quad at \quad x = x_{\max} \quad (x_{\max} > t)$$

The last boundary condition of eq. (16) is needed if the first right-hand-side term of eq. (6) is significant and x_{max} is larger than t. If reference is made to steady state conditions, then the last boundary condition should be replaced by

$$\frac{\partial C}{\partial x} \to 0 \quad at \quad x = x_{\max} \quad (x_{\max} < t) \tag{17}$$

As interest was concentrated on the penetration of the salinity into the domain of eq. (9) and build-up of the ROI, besides the boundary conditions of eq. (16) we had to consider the following initial conditions

$$\begin{aligned} &C = 0 \quad at \quad t = 0,\ x, y \geq 0 \quad except\ for\ the\ point\ x, y = 0 \\ &C = 0.5\ at \quad x, y = 0 \end{aligned} \tag{18}$$

We applied the TSBL method to development of a quantitative modeling approach describing the salinity distribution and build-up of the ROI in the domain of eq. (9). Fig. 2 represents the basic domain structure of the salinity distributions.

It was assumed that the salinity profile, at each cross-section perpendicular to the x-axis, could be described by a combination of two boundary layers (BLs) taking place in adjacent ranges of the y coordinate. The inner BL was represented by the salinity distribution:

$$C = C_b\left[1 - (1 - c_r)(1 - \xi)^{n_1}\right];\ \xi = \frac{\delta_u - y}{\delta_u};\ 0 \leq y \leq \delta_u \tag{19}$$

where n_1 is a power coefficient; ξ is the inner BL coordinate; c_r is the ratio between the salinity at $y = \delta_u$ and the salinity C_b, at $y = 0$.

The outer BL was represented by the salinity distribution

$$C = c_r C_b (1 - \eta)^{n_2};\ \eta = \frac{y - \delta_u}{\delta_0 - \delta_u};\ \delta_u \leq y \leq \delta_0 \tag{20}$$

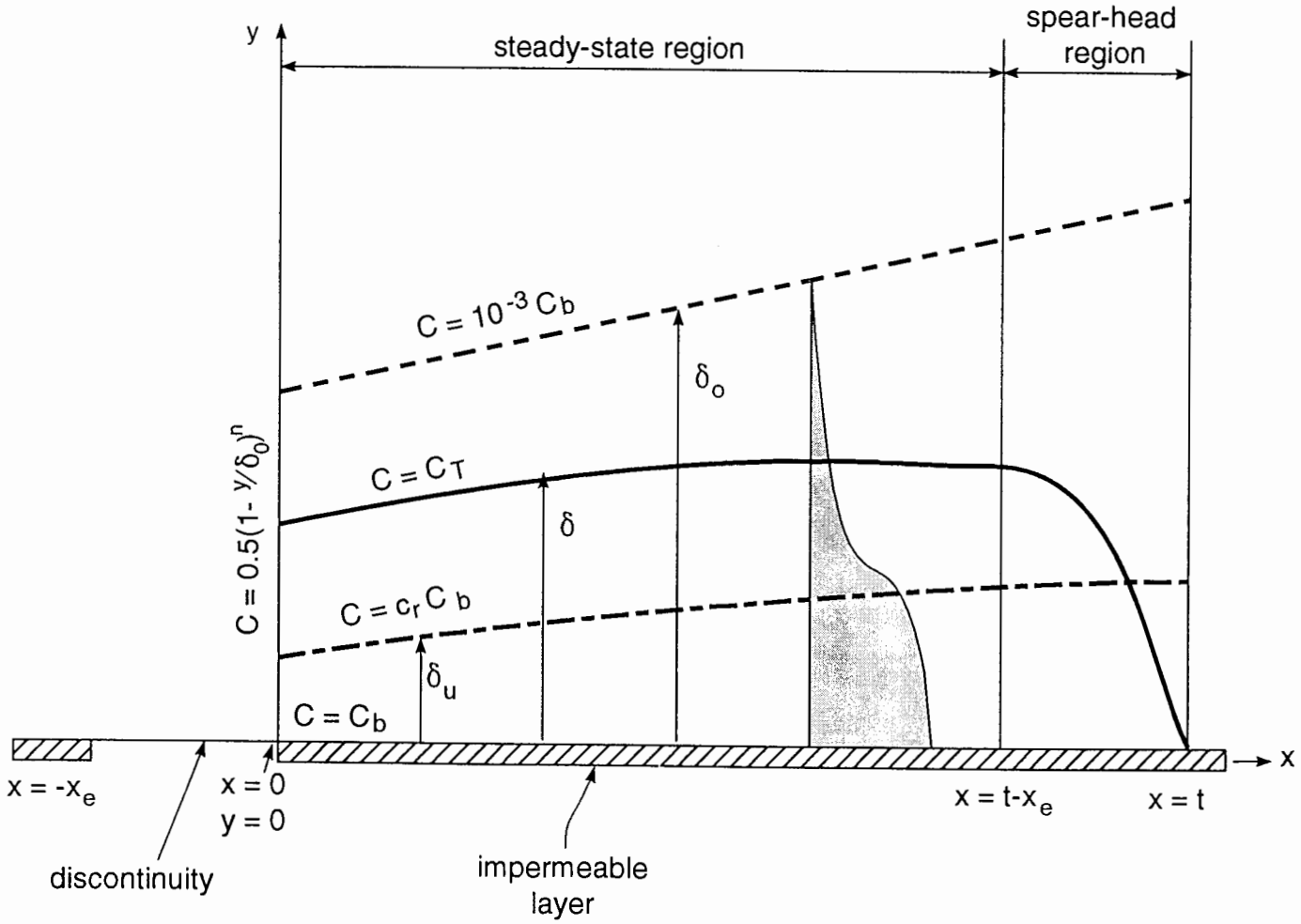

Fig. 2. Schematics depicting salinity values at the domain boundaries as well as at the edges of the inner (δ_u), outer (δ_0), and top-specified (δ) boundary layers.

where n_2 is a power coefficient; η is the outer BL coordinate.

We were especially interested in the identification of a possible constant value of c_r associated with negligible salinity transfer between the two BLs specified by eqs. (19) and (20), respectively. We adopted this approach following numerous numerical experiments in which we solved eq. (6) subject to the boundary and initial condition of eqs. (13)–(18). In these experiments we calculated salinity fluxes through isohalines normalized with regard to C_b values the results showed very minor salinity fluxes from the inner BL into the outer one. Therefore, we decided to identify the value of the normalized isohaline, c_r, associated with the minimum and almost negligible salinity flux crossing that normalized isohaline.

We applied the principle of mass conservation between the left and right hand sides of $x = 0$, assuming an identical contaminant mass flux between the impermeable layer and $y = \delta_u$ on both sides of $x = 0$. Therefore, there were also identical fluxes through the portions of the aquifer located between δ_u and δ_0 on both sides of $x = 0$. These conditions yielded:

$$\{C_b \delta_u\}_{right} = \frac{(n_1+1)\left(1-0.5^{(n+1)/n}\right)}{(n+1)(n_1+0.5)} \{C_b \delta_0\}_{left} \tag{21a}$$

$$\{C_b(\delta_0 - \delta_u)\}_{right} = \frac{2 \times 0.5^{(n+1)/n}(n_2+1)}{(n+1)} \{C_b \delta_0\}_{left} \tag{21b}$$

where subscripts *left* and *right* refer to left and right hand sides of $x = 0$, respectively. It should be noted that C_b at the left hand side of $x = 0$, was 0.5

Equations (21a) and (21b) incorporate 3 unknown quantities at the right hand side of $x = 0$, namely C_b, δ_u and δ_0. Some numerical experiments showed that it was appropriate to keep the value of δ_0 unchanged, and to modify values of the other two parameters. However, obtained changes of the values of C_b and δ_u were minor.

The ROI was considered as a top specified boundary layer (TSBL). At the top of the ROI

$y = \delta$, and the value of C was C_T, where C_T was the acceptable value of salinity, namely C_T = 0.005 as considered by Rubin and Buddemeier (1998a).

Continuity of the slope of the salinity profile at $y = \delta_u$ required, according to eqs. (19) and (20),

$$\frac{\delta_0}{\delta_u} = \frac{c_r n_2}{(1-c_r)n_1} + 1 \tag{22}$$

Conservation of mass implied for the inner boundary layer

$$\frac{\partial}{\partial t}\left(\int_0^{\delta_u} C dy\right) + \frac{\partial}{\partial x}\left(\int_0^{\delta_u} C dy\right) = 0 \tag{23}$$

Referring to a moving coordinate system we obtain

$$\frac{d}{dt}(C_b \delta_u) = 0 \tag{24a}$$

Therefore

$$(C_b \delta_u)_{x,t} = (C_b \delta_u)_{x=0, t_0 = t-x} \tag{24b}$$

We considered that the vertical salinity gradient did not lead to salinity transport between the inner and outer BLs, but led to the expansion of the two BLs. Therefore, we obtained for the inner BL

$$C_{avu} \frac{d\delta_u}{dt} = -\alpha_1 a \left(\frac{\partial C}{\partial y}\right)_{y=\delta_u} \tag{25}$$

where α_1 is a coefficient; C_{avu} is the average salinity of the inner BL

$$C_{avu} = \frac{1}{\delta_u}\int_0^{\delta_u} C dy \tag{26}$$

Introducing eq. (19) into eq (26) we obtained

$$C_{avu} = C_b \frac{n_1 + c_r}{n_1 + 1} \tag{27}$$

Considering that at the left hand side of $x = 0$ the value of C_b was 0.5, we applied eq. (13) to obtain for the left-hand side of x=0:

$$\left(\frac{\delta_u}{\delta_0}\right)_{x=0} = 1 - c_r^{\frac{1}{n}} \tag{28}$$

It should be noted that eq. (22) refers to the calculation of quantities at the right-hand side of $x = 0$. However, often the difference between results of eqs. (21) and (28) are minor.

Introducing eqs. (19) and (27) into eq. (25) we obtained

$$\frac{d\delta_u^2}{dt} = \alpha_1 \frac{2a(1-c_r)n_1(n_1+1)}{n_1 + c_r} \tag{29}$$

Direct integration of this expression yielded

$$\left(\delta_u^2\right)_{x,t} = \left(\delta_u^2\right)_{x=0,t_0=t-x} + \alpha_1 \frac{2a(1-c_r)n_1(n_1+1)}{n_1 + c_r} x \tag{30}$$

Equations (14), (28), (30), and (24) fully determine the distribution of δ_u and C_b in the domain.

Equations (14), (28), and (24) implied that eq. (30) could be used at

$$0 \le x \le t \tag{31}$$

For $x > t$ the BLs vanished.

Steady state conditions were established in the region where

$$0 \le x \le t - x_e \tag{32}$$

provided that $t > x_e$

Principles similar to those leading to eqs. (22)–(30), were also used with regard to the outer BL.

We again considered that salinity gradients in the outer BL led to its expansion and obtained

$$C_{avo}\frac{d}{dt}(\delta_0-\delta_u)=-\alpha_2 a\left(\frac{\partial C}{\partial y}\right)_{y=\delta_u} \tag{33}$$

where α_2 is a coefficient; C_{avo} is the average salt concentration in the outer BL.

$$C_{avo}=\frac{1}{\delta_0-\delta_u}\int_{\delta_u}^{\delta_0}C dy \tag{34}$$

Introducing eq. (20) into eq. (34) we obtained:

$$C_{avo}=C_b\frac{c_r}{n_2+1} \tag{35}$$

Introducing eqs. (20) and (35) into eq. (33) we obtained:

$$\frac{d}{dt}(\delta_0-\delta_u)^2=2\alpha_2 a n_2(n_2+1) \tag{36}$$

Direct integration of this expression and reference to the initial and boundary conditions of eqs. (14) and (21) or (28) yielded:

$$(\delta_0-\delta_u)^2_{x,t}=(\delta_0-\delta_u)^2_{x=0,t_0=t-x}+2\alpha_2 a n_2(n_2+1)x \tag{37}$$

Again, only x-values smaller than t should be considered.

Following the determination of δ_u, Cb and δ_0, the thickness, δ, of the ROI defined as the top specified boundary layer, could be calculated. The value of this parameter was associated with the isohaline $C = C_T$. The value of δ could be either in the range of y values at the outer BL, provided that $C_T < c_r C_b$, or at the inner BL, provided that $C_T > c_r C_b$.

If $\delta_u < \delta < \delta_0$ then according to eq. (20)

$$C_T=c_r C_b(1+\eta_T)^{n_2} \tag{38}$$

where η_T is associated with the value of $y = \delta$.

Equation (38) yielded:

$$\eta_T=1-\left(\frac{C_T}{c_r C_b}\right)^{\frac{1}{n_2}} \tag{39}$$

$$\delta = \eta_T(\delta_0 - \delta_u) + \delta_u \tag{40}$$

If $0 < \delta < \delta_u$ then according to eq. (19)

$$C_T = C_b\left[1-(1-c_r)(1-\xi_T)^{n_1}\right] \tag{41}$$

where ξ_T is associated with the value $y = \delta$.

Equation (41) yielded

$$\xi_T = 1-\left(\frac{1-C_T/C_b}{1-c_r}\right)^{\frac{1}{n_1}} \tag{42}$$

$$\delta = \delta_u(1-\xi_T) \tag{43}$$

Equations (14), (21), (28), (30), (24), (37), and (40) or (43) provided a complete closed form analytical solution for the determination of δ_u, C_b, δ_0 and δ. Thereby, salinity transport and distribution in the domain $x, y \geq 0$ was fully determined, and the build-up of the ROI could be followed.

The general method of calculation given in this section seems quite simple and attractive. However, it required some preliminary tests indicating that:

1) It was possible to divide salinity profiles into two BLs;
2) There was negligible salt mass transfer between the two BLs;
3) Salinity profiles in each BL obeyed some laws of similarity; and
4) The ratio between the thickness of the two BLs became constant at a certain comparatively small value of x.

The following section reports the performance and evaluation of some preliminary tests aimed at the consideration of these issues.

Preliminary Tests

We were especially interested in the identification of a possible constant value of c_r associated with negligible salinity transfer between the two BLs specified by eqs. (19) and (20),

respectively. We adopted this approach following numerous numerical experiments in which we solved eq. (6) subject to the boundary and initial condition of eqs. (13)–(18). In these experiments we calculated salinity fluxes through isohalines normalized with regard to C_b values the results showed very minor salinity fluxes from the inner BL into the outer one. Therefore, we decided to identify the value of the normalized isohaline, c_r, associated with the minimum and almost negligible salinity flux crossing that normalized isohaline.

During the process of build-up of the salinity profile at $x = 0$, as given by eq. (14), it seemed that a spearhead front of salinity penetrated into the domain $x, y \geq 0$ from its left-hand-side boundary. At the penetrating front of the salinity some longitudinal dispersion probably took place. Longitudinal dispersion probably had also some effect at the left-hand-side boundary of the domain, where the salinity profile was adopted from Dirichlet-type boundary conditions at $y = 0$, $-x_e \leq x \leq 0$ to Neumann type with zero flux at $y = 0$, $x > 0$. This phenomenon was represented by the transition from the relationship given by eq. (28) to that given by eq. (21). However, for most parts of the domain $x, y \geq 0$ we might assume that longitudinal dispersion effects were very minor in comparison to salinity advection in the longitudinal direction.

Calculations of the preceding section indicated that steady state conditions gradually developed in the simulated domain $x, y \geq 0$. If we referred to a limited region of the domain $0 \geq x \geq x_{max}$ where $x_{max} < t-x_e$ then this region was subject to steady state conditions. As a preliminary set of tests we considered it appropriate to refer to all issues identified at the end of the preceding section by comparing the BL solution approach with the solution of the steady state version of eq. (6), in which effects of longitudinal dispersion were ignored. Therefore, the reference was to the differential equation

$$\frac{\partial C}{\partial x} = a\frac{\partial^2 C}{\partial y^2} \tag{44}$$

This equation was subject to the relevant boundary conditions of eqs. (12) and (16), namely

$$\frac{\partial C}{\partial y} = 0 \quad at \quad y = 0$$
$$C \to 0 \quad at \quad y \to \infty \tag{45}$$
$$C = 0.5 erfc\left(\frac{y}{2\sqrt{ax_e}}\right) \quad at \quad x = 0$$

The problem of salinity transport represented by eqs. (44) and (45) is analogous to heat conduction in an insulated semi-infinite domain subject to an initial temperature distribution. Therefore, various analytical solutions associated with some numerical integration could be useful to solve this problem (Carslaw & Jaeger, 1959; Hill and Dewynne, 1987). Also at very large distances from the discontinuity exposure, namely if $x>>x_e$, the exposure could be considered as a point source, whose strength could be obtained by integrating the salinity flux over the exposure. Then by using the image method (e.g. Fischer et al., 1979), the salinity distribution in the domain could be obtained. It should, however, be noted that the analytical and semi-analytical methods, mentioned in preceding phrases, require reference to completely homogeneous domains. On the other hand the BL approach allows reference to domains, which are not necessarily homogeneous in the longitudinal direction. Though we have performed various types of tests of the BL approach, only a summary of our tests, performed by numerical simulations are brought in this paper.

In the framework of our numerical simulation tests, we have applied the following Crank-Nicolson implicit finite difference scheme

$$\begin{aligned} &-C_{r+1,s-1}\frac{a\Delta x}{2(\Delta y)^2} + C_{r+1,s}\left[1+\frac{a\Delta x}{(\Delta y)^2}\right] - C_{r+1,s+1}\frac{a\Delta x}{2(\Delta y)^2} \\ &= C_{r,s-1}\frac{a\Delta x}{2(\Delta y)^2} + C_{r,s}\left[1-\frac{a\Delta x}{(\Delta y)^2}\right] + C_{r,s+1}\frac{a\Delta x}{2(\Delta y)^2} \end{aligned} \tag{46}$$

where r and s represent nodal point numbers in the x and y directions, respectively.

Figure 3 shows how the steep salinity profile at $x = 0$ progressively became shallower with increasing values of x. The decrease of the vertical salinity gradient was associated with

penetration of the salinity to increasing values of the y coordinate. This penetration was more significant for larger dispersivity values.

Figure 4 provides information about the variation of C_b with the x coordinate. Various values of the dispersivity, a, and the exposure, x_e, were considered.

Figure 5 compares profiles of C_b obtained with various x_e-values and a single dispersivity. We have performed numerous experiments to determine possible values of c_r and n_2. In these experiments values of δ_u and δ_0 have been identified for various x-values (see Fig. 2). Then we calculated the value of

$$\delta_R = \delta_0 / \delta_u \tag{47}$$

By introducing the value of this parameter and a best fit value of n_2 into eq. (22) the value of n_1 was calculated.

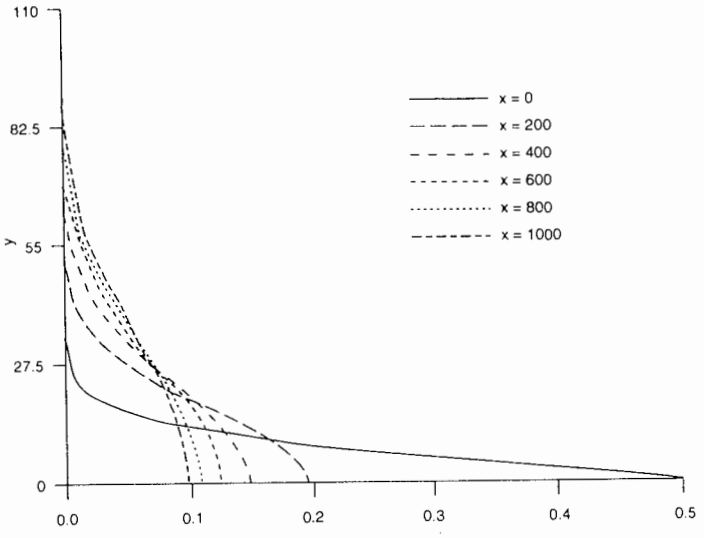

Figure 3(a)

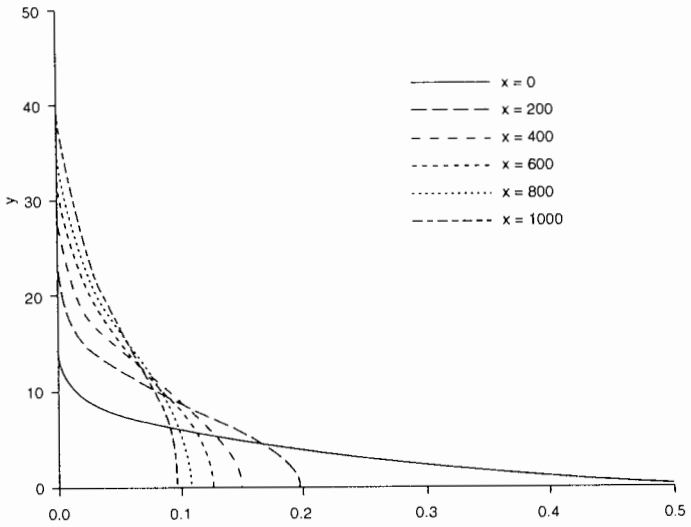

Figure 3(b)

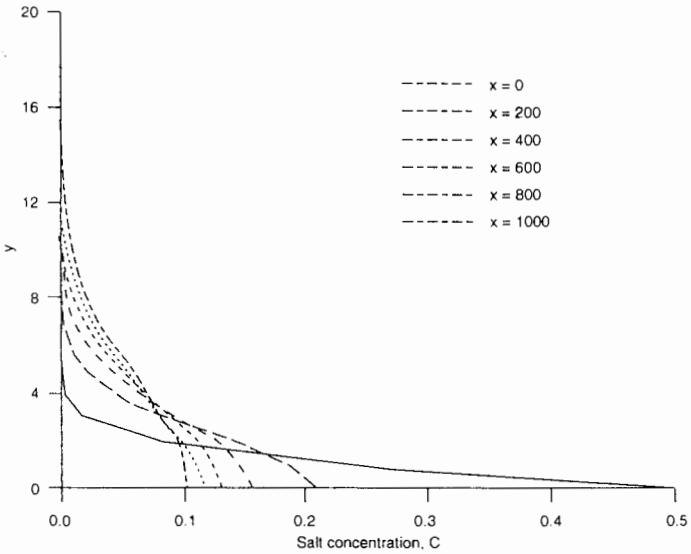

Figure 3(c)

Fig. 3. Steady state salinity profiles at various x-values ($x_e = 100$)

(a) $a = 0.5$ (b) $a = 0.1$ (c) $a = 0.01$

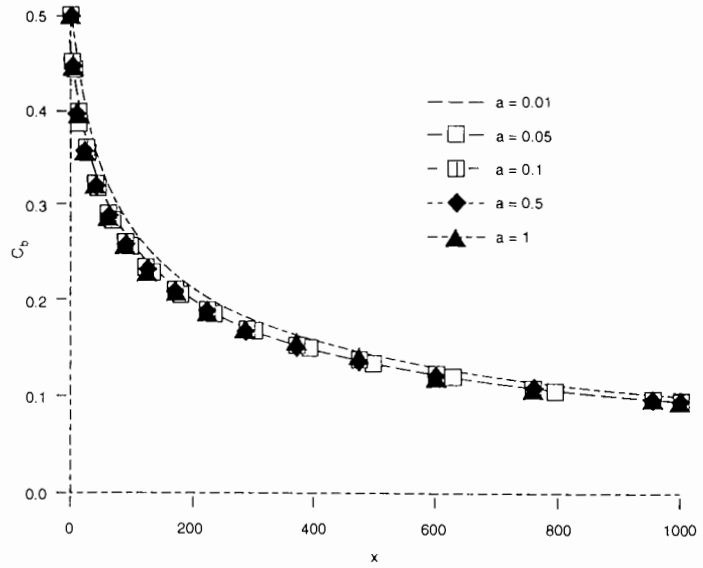

Figure 4(a)

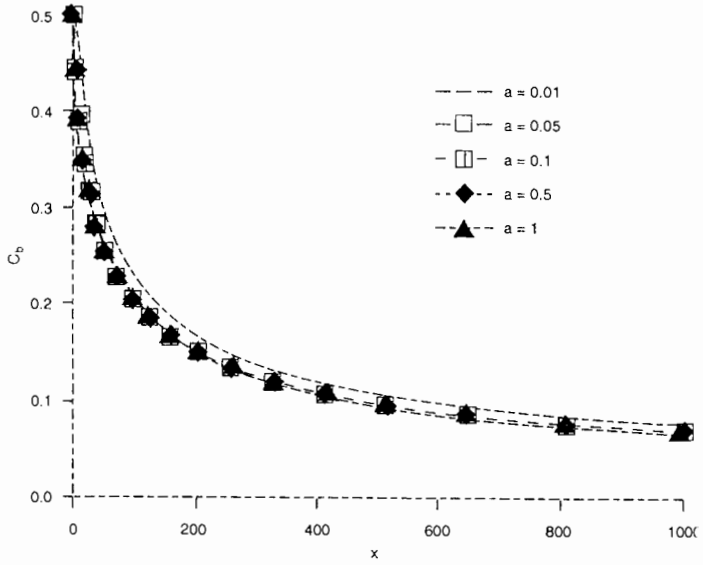

Figure 4(b)

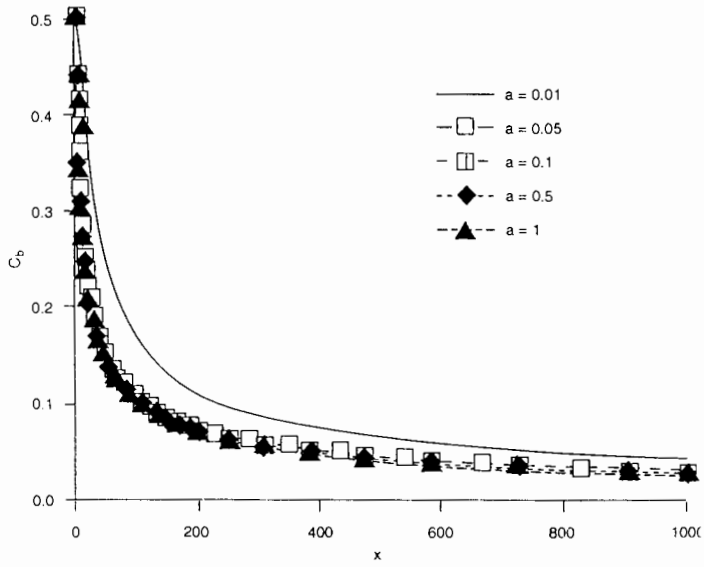

Figure 4(c)

Fig. 4. Profiles of C_b for various values of a

(a) $x_e = 100$ (b) $x_e = 50$ (c) $x_e = 10$

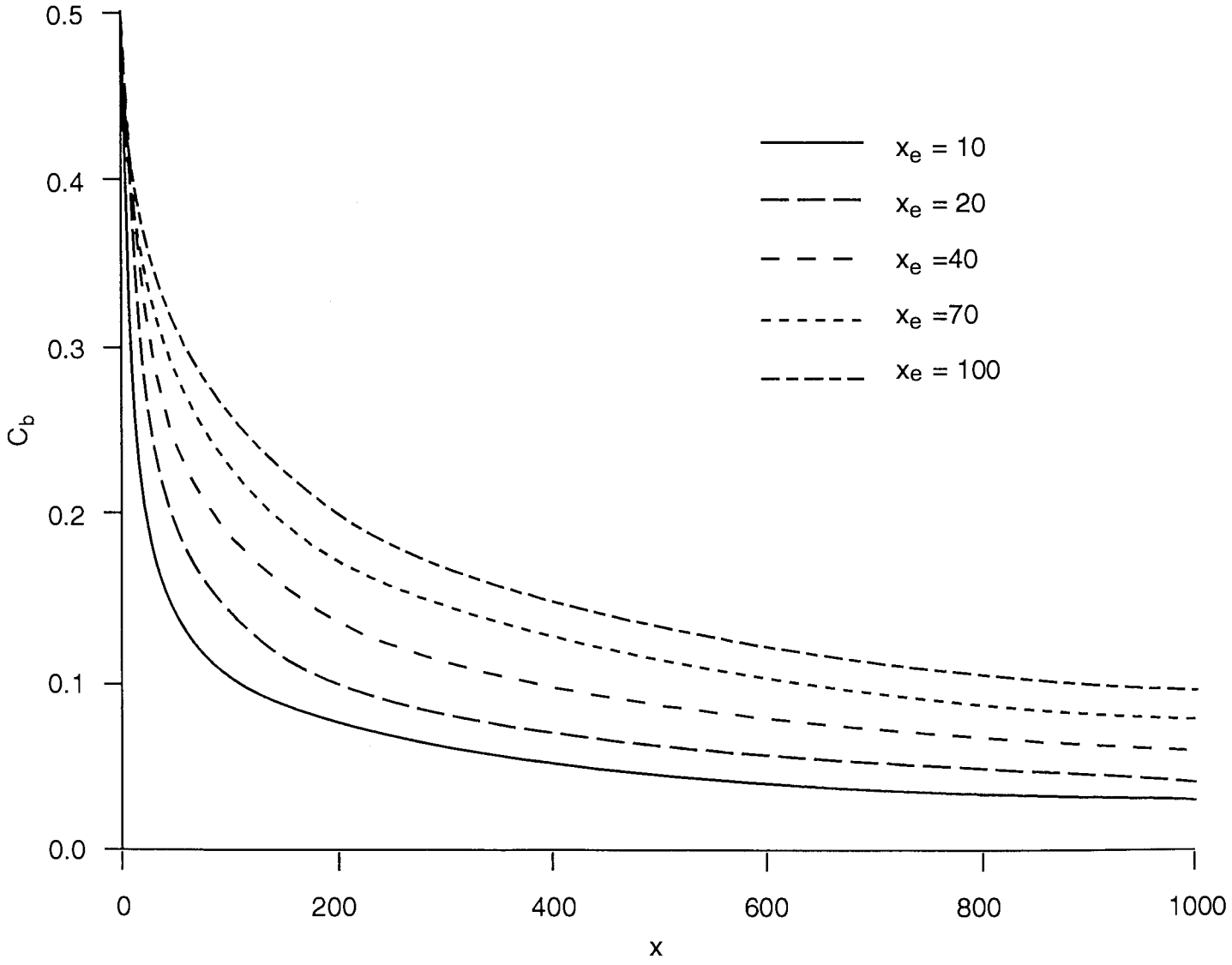

Fig. 5. Profiles of C_b for various x_e-values ($a = 0.1$)

Our numerical experiments showed that a very reasonable value for c_r was:

$$c_r = 0.5 \tag{48}$$

We have also found best fit of salinity profiles when considering

$$n_2 = 4 \tag{49}$$

Figure 6 shows how the value of δ_R changed in a short distance from the quantity defined by eq. (28) to a constant value independent of x. When the constant value of δ_R was established then n_1 also reached a constant value. We also found best fit values of α_1 and α_2

$$n_1 = 1.84; \quad \alpha_1 = 0.935; \quad \alpha_2 = 0.775 \tag{50}$$

Both coefficients, α_1 and α_2 were found to be quite close to unity.

Our experiments have been performed for quite wide ranges of the parameters x_e and a:

$$\begin{aligned} 10 \le x_e \le 100 \\ 0.01 \le a \le 1.0 \end{aligned} \tag{51}$$

For the ranges of values given by eq. (51) best fit values for the salinity profile were identical to those given by eq. (48)–(50), as shown in Fig. 7. In this figure we have presented the numerically calculated C profiles at x = 500, 1000 as a check on the adequacy of eqs. (19) and (20) as well as (22) with various values of n_2. The values given by eqs. (49) and (50) provided the best fit C -profiles when a = 0.5 and x_e = 100.

Figure 8 exemplifies the tests considering the applicability of the BL approach for a = 0.1, x_e = 100 and different x-values. Fig. 8 eventually indicates that for the range of x-values

$$10 \le x \le 1000 \tag{52}$$

the BL approach of this study with quantities given by eqs. (48)–(50) provided a quite accurate description of salinity transport and distribution in the domain of $x, y \ge 0$. We have not observed any limitation on the maximum value of x to which the BL approach could be applied.

In the next stage we have compared the steady state simulations obtained by using eq. (44) with those obtained by using the BL approach with quantities given by eqs. (48)–(50).

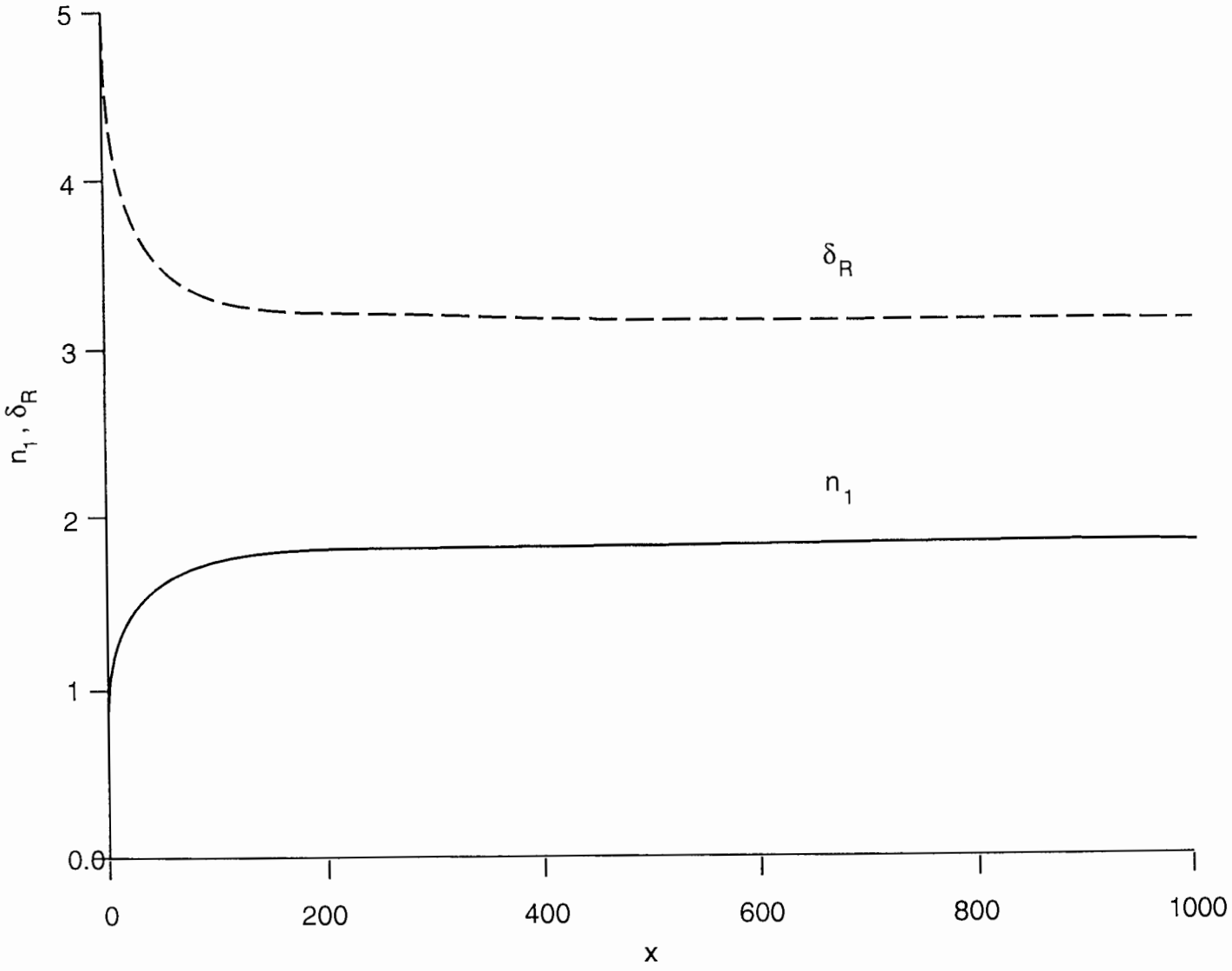

Fig. 6. Values of δ_R and n_1 versus x ($a = 0.1$, $x_e = 100$, $n2 = 4$)

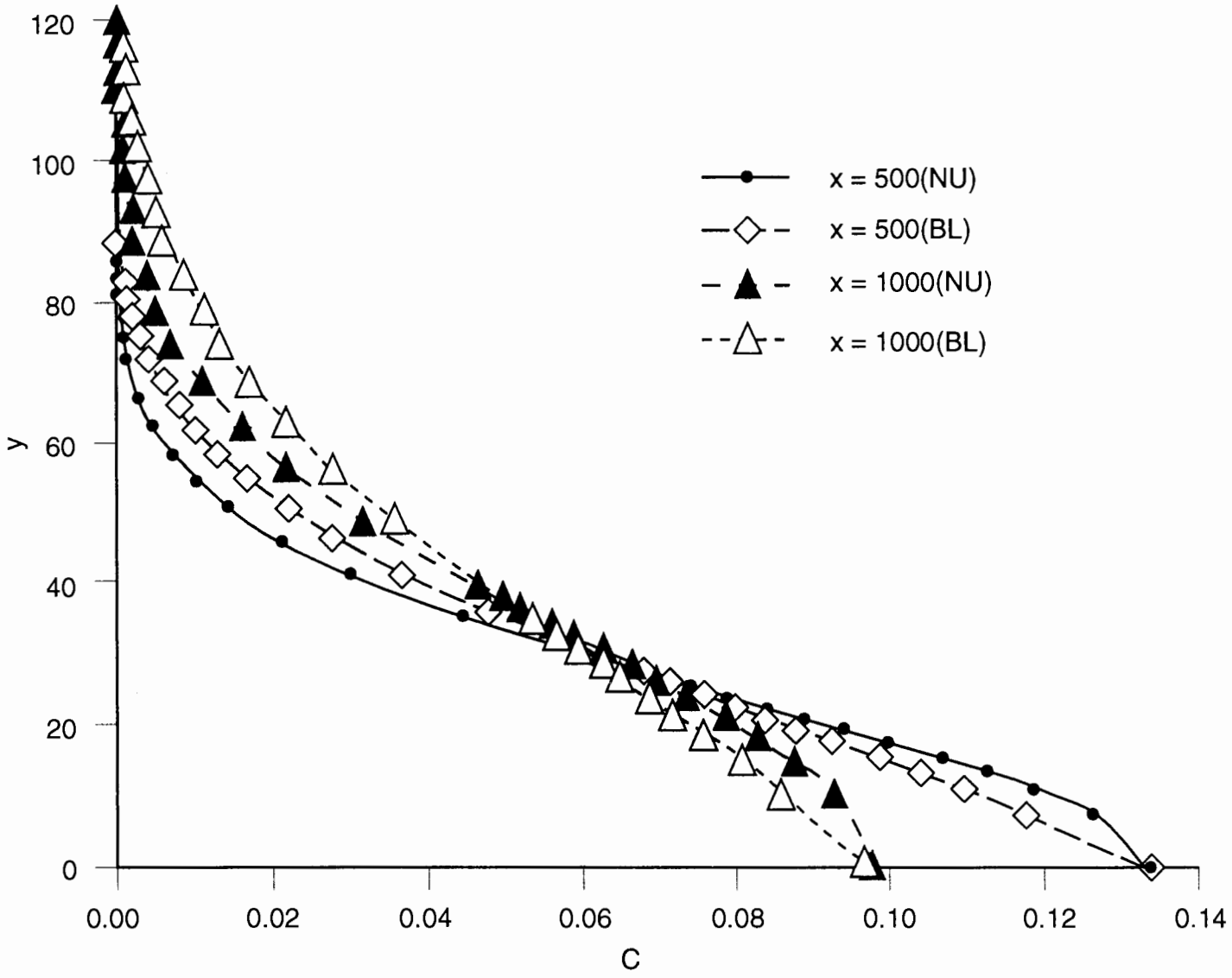

Fig. 7a Determination of the value of n_2; NU = numerical simulation; BL = boundary layer calculation.

($a = 0.5$, $x_e = 100$, $c_r = 0.5$)

(a) $n_2 = 3$

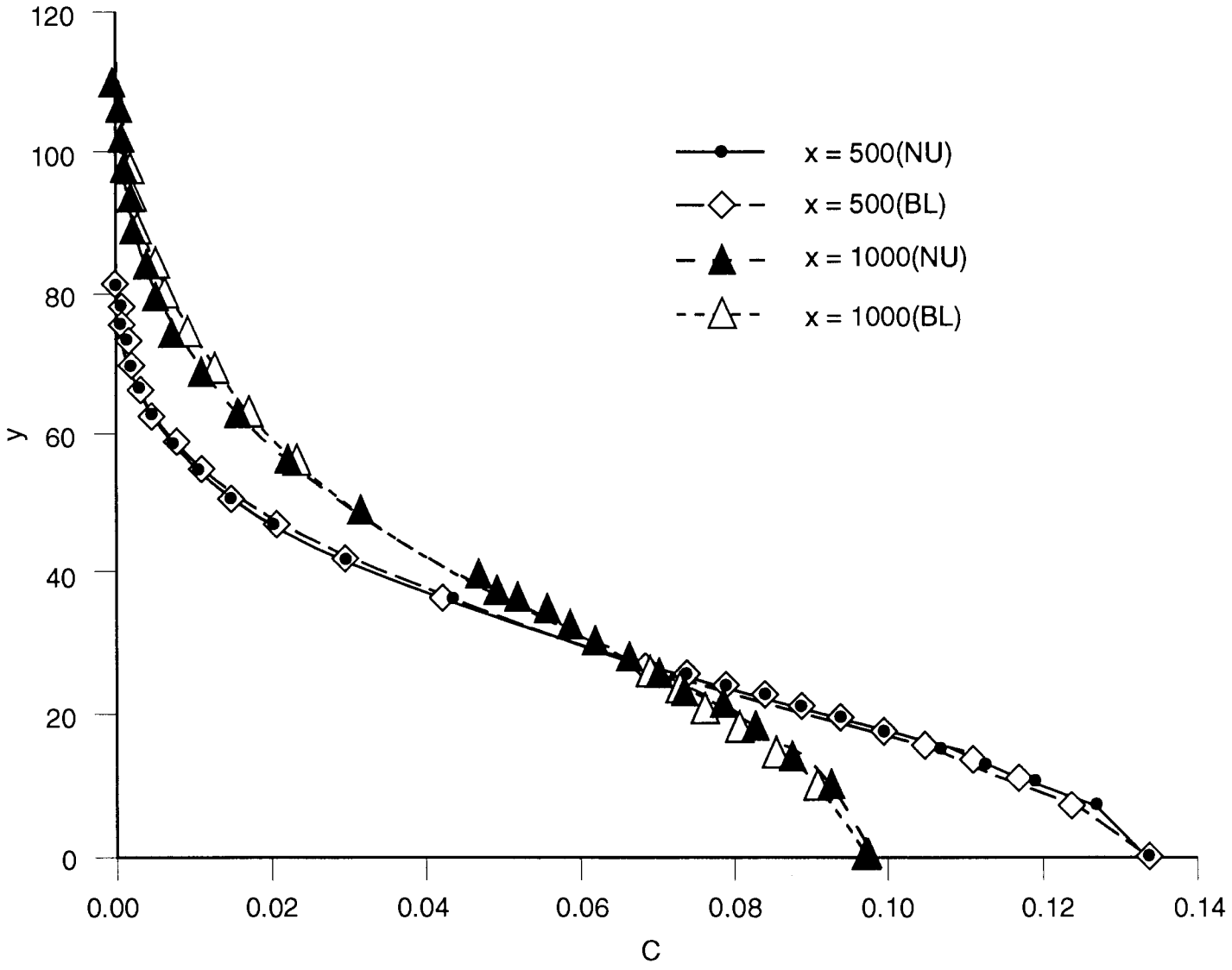

Fig. 7b Determination of the value of n_2; NU = numerical simulation; BL = boundary layer calculation.

($a = 0.5$, $x_e = 100$, $c_r = 0.5$)

(b) $n_2 = 4$

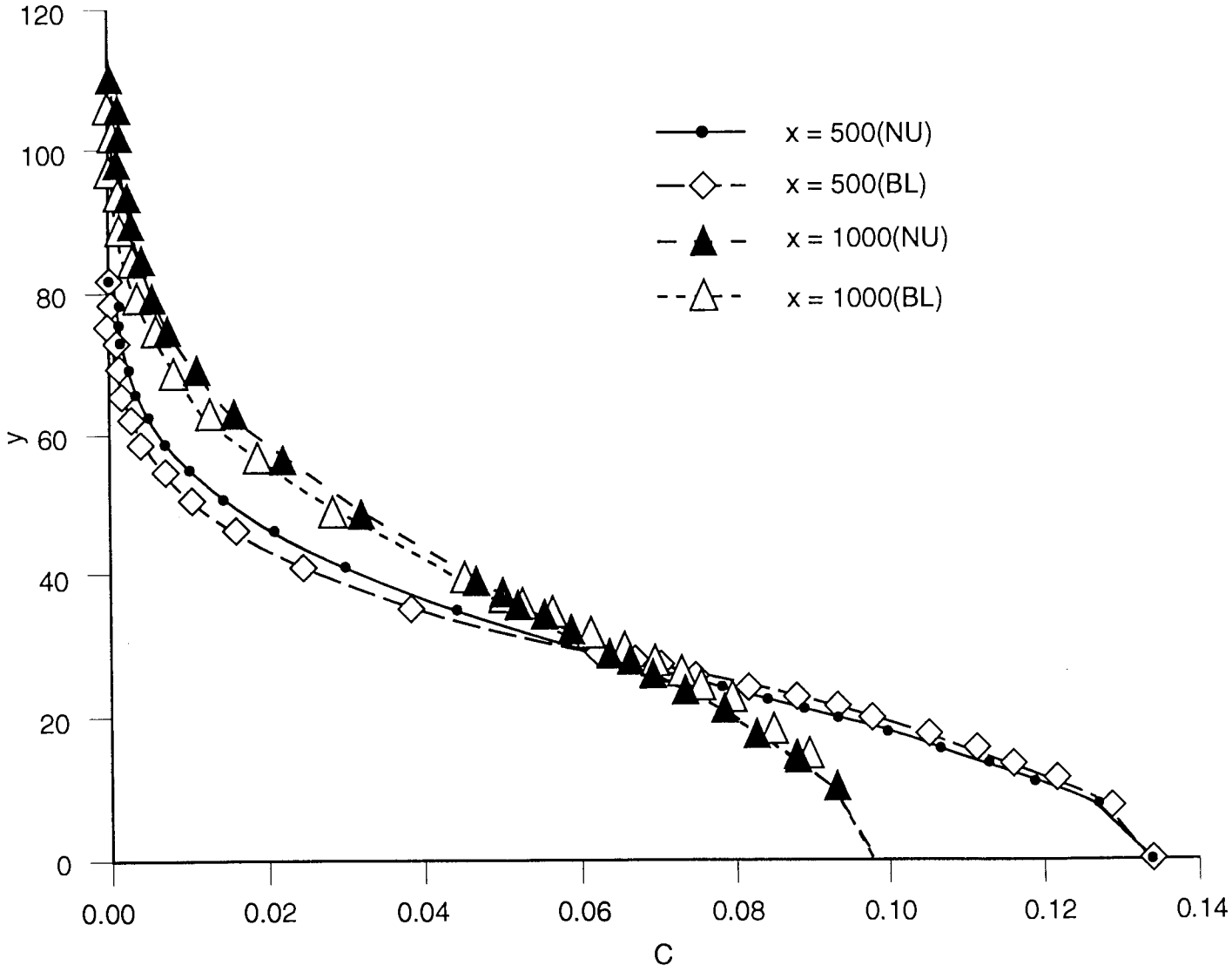

Fig. 7c Determination of the value of n_2; NU = numerical simulation; BL = boundary layer calculation.

($a = 0.5$, $x_e = 100$, $c_r = 0.5$)

(c) $n_2 = 5$

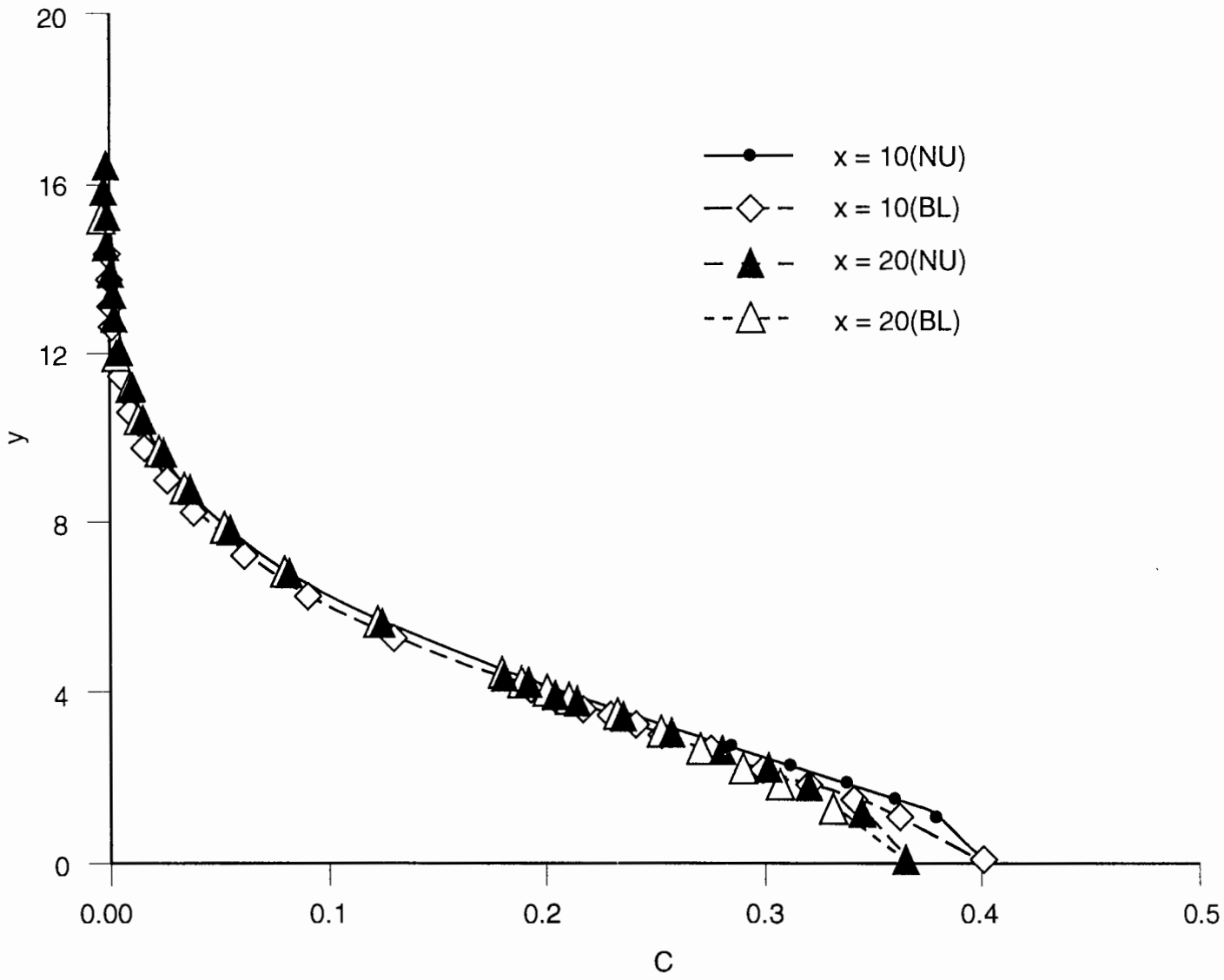

Fig. 8. Comparisons of profiles of C versus y at various x-values; NU = numerical simulation; BL = boundary layer calculation.

($a = 0.1$, $x_e = 100$, $n_2 = 4$).

(a) $x = 10, 20$

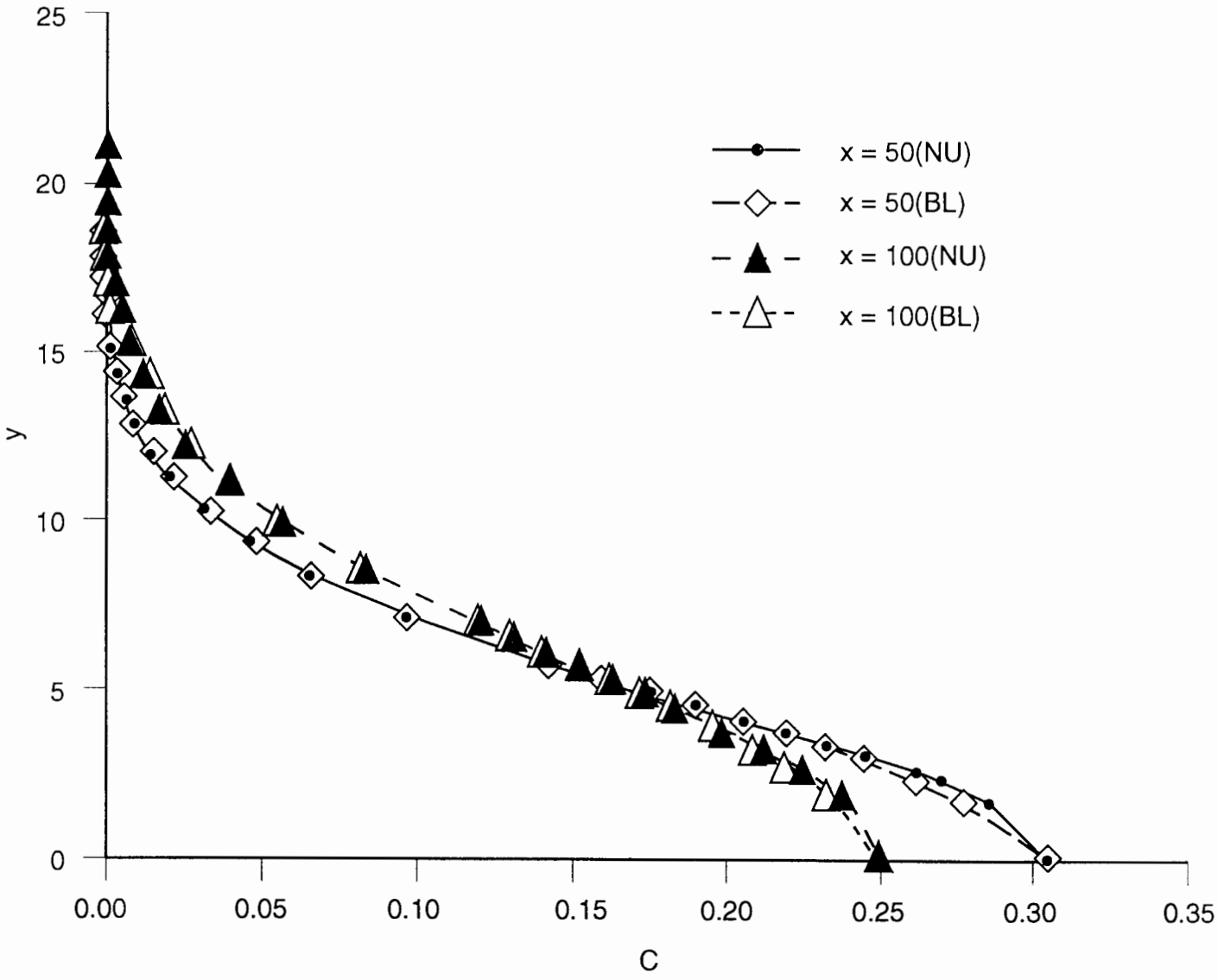

Fig. 8b Comparisons of profiles of C versus y at various x-values; NU = numerical simulation;

BL = boundary layer calculation.

(b) $x = 50, 100$

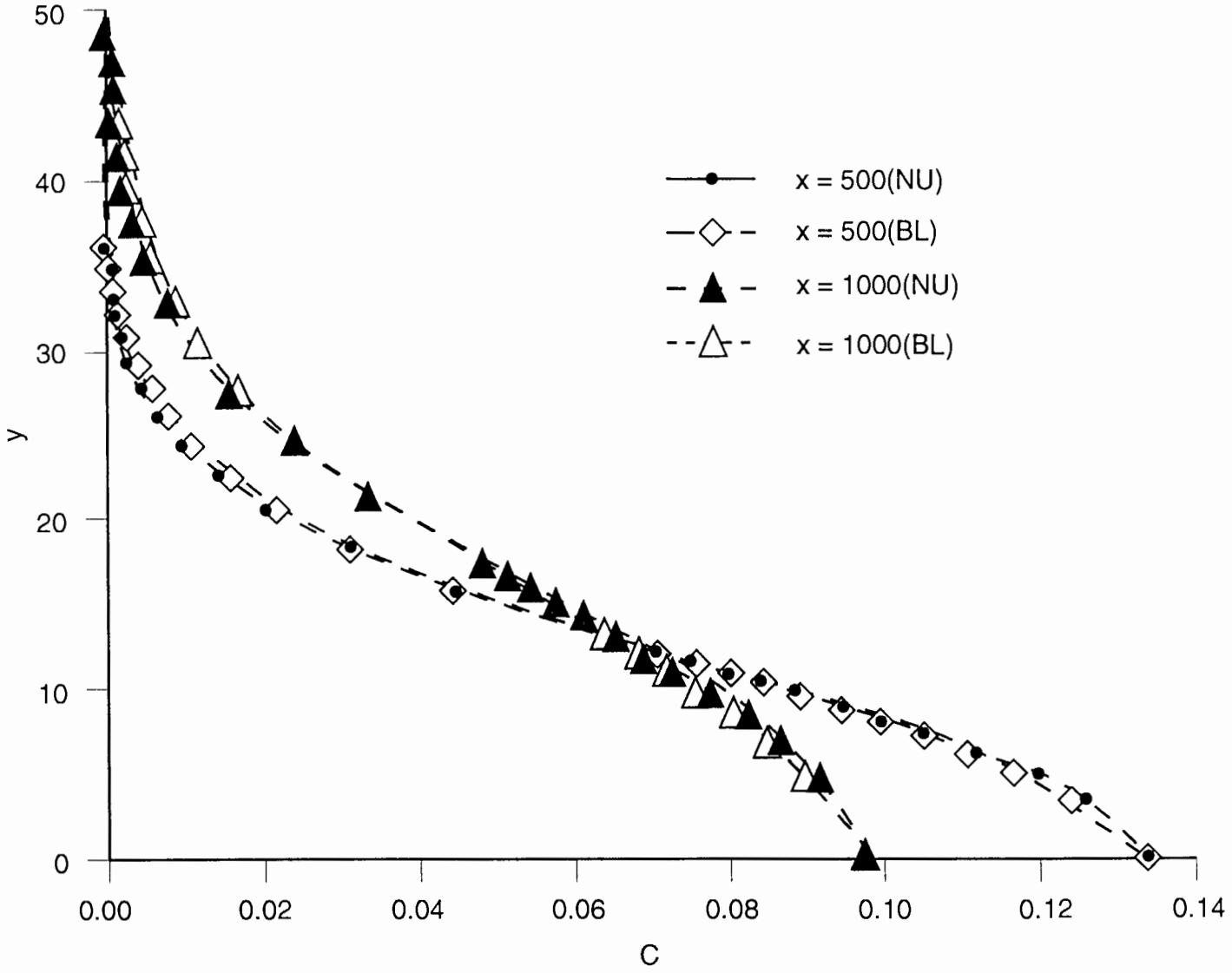

Fig. 8c Comparisons of profiles of C versus y at various x-values; NU = numerical simulation;

BL = boundary layer calculation.

($a = 0.1$, $x_e = 100$, $n_2 = 4$).

(c) $x = 500$, 1000

Figure 9 provides a comparison between values of δ_u, δ and δ_0 obtained by both methods. Generally, differences between values of the various parameters were not significant, and they were definitely acceptable from the point of view of practical application.

Figure 10 provides a comparison between steady state profiles of C_b obtained by applying eq. (44) and those obtained by using the BL approach with quantities given by eqs. (48)-(50). Again, differences were small.

Characterizing the Mineralization Process

Equation (14) indicated that the boundary condition at the left hand side of the domain $x, y \geq 0$ was subject to changes until $t = x_e$. Therefore, for t-values larger than x_e we identified in the domain two regions as represented by Fig. 11: (a) the spearhead region associated with the penetrating salt front at $t - x_e \leq x \leq t$, and (b) the steady state region at $0 \leq x \leq t - x_e$.

As indicated by eqs. (30) and (37) as well as Fig. 11, values of δ_u and δ_0 progressively increase with x. The expansion of these layers decreases their average salinity. Therefore, the value of δ, associated with a constant salinity value $C = C_T$ did not increase at the same rate as δ_0 and δ_u, as illustrated in Fig. 2.

The spearhead region represents the first x_e units of the salinity penetration into the aquifer. Fig. 11(a) shows the BLs for $t = 100$; since this is the value of x_e, the entire region consists of the spearhead. In this case the value of δ decreased only over the last twenty units of the x-values, namely at $80 \leq x \leq 100$. Fig. 11(b) displays the case of $t = 1000$. The salinity penetration is shown for the spearhead region as well as the steady state region. Fig. 11(c) shows the various boundary layers in the spearhead region only for $t = 1000$. In this case the value of δ decreases along the whole spearhead region.

Figure 12 indicates that the decrease in values of δ with increasing x-values is limited to the spearhead region even at a significant distance from the discontinuity in the impermeable layer. Fig. 13 shows conditions at a very large distance from the discontinuity. However, again

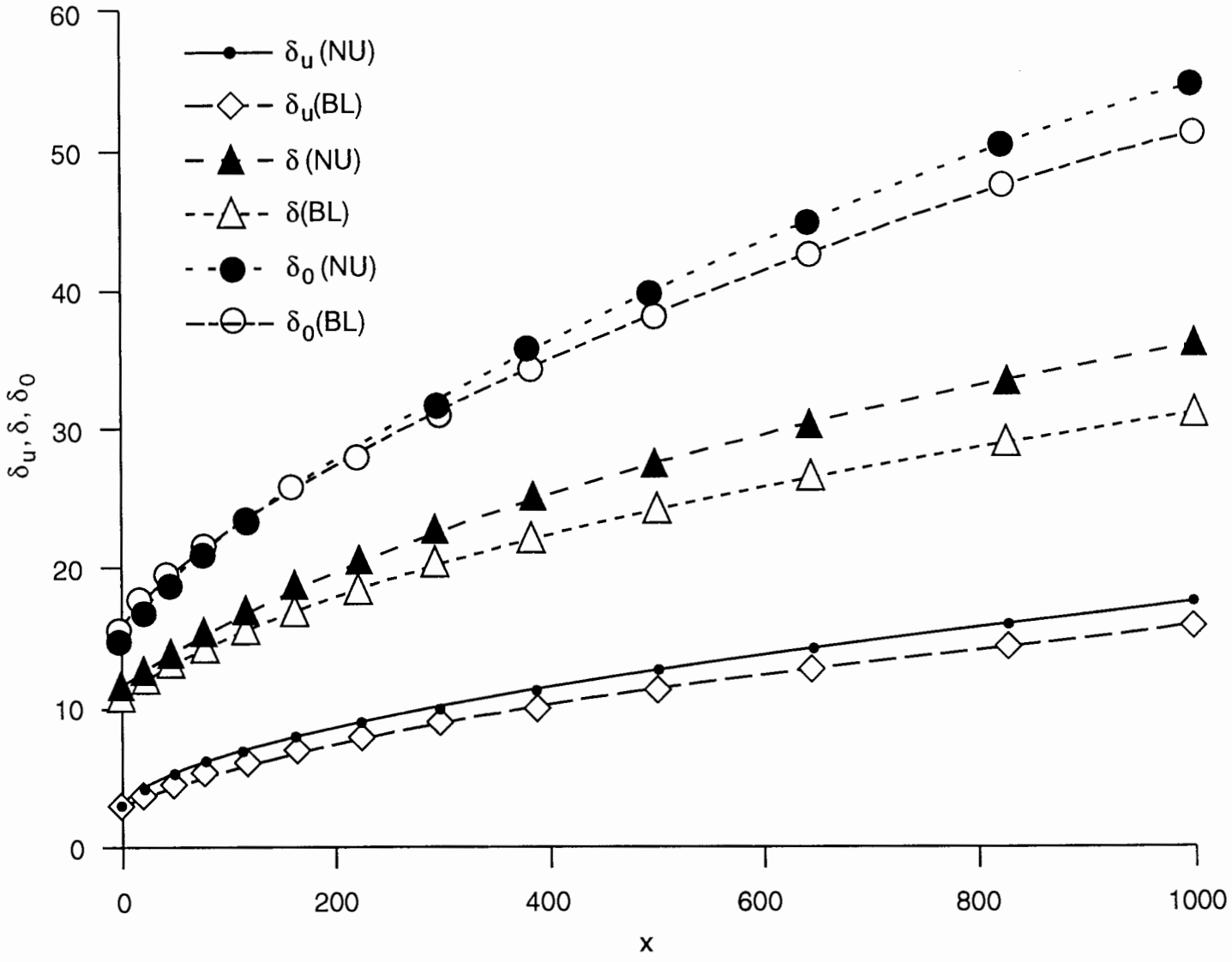

Fig. 9 Comparisons of steady state values of BL thicknesses obtained from numerical simulation (NU) and boundary layer calculation (BL). ($a = 0.1$, $x_e = 100$)

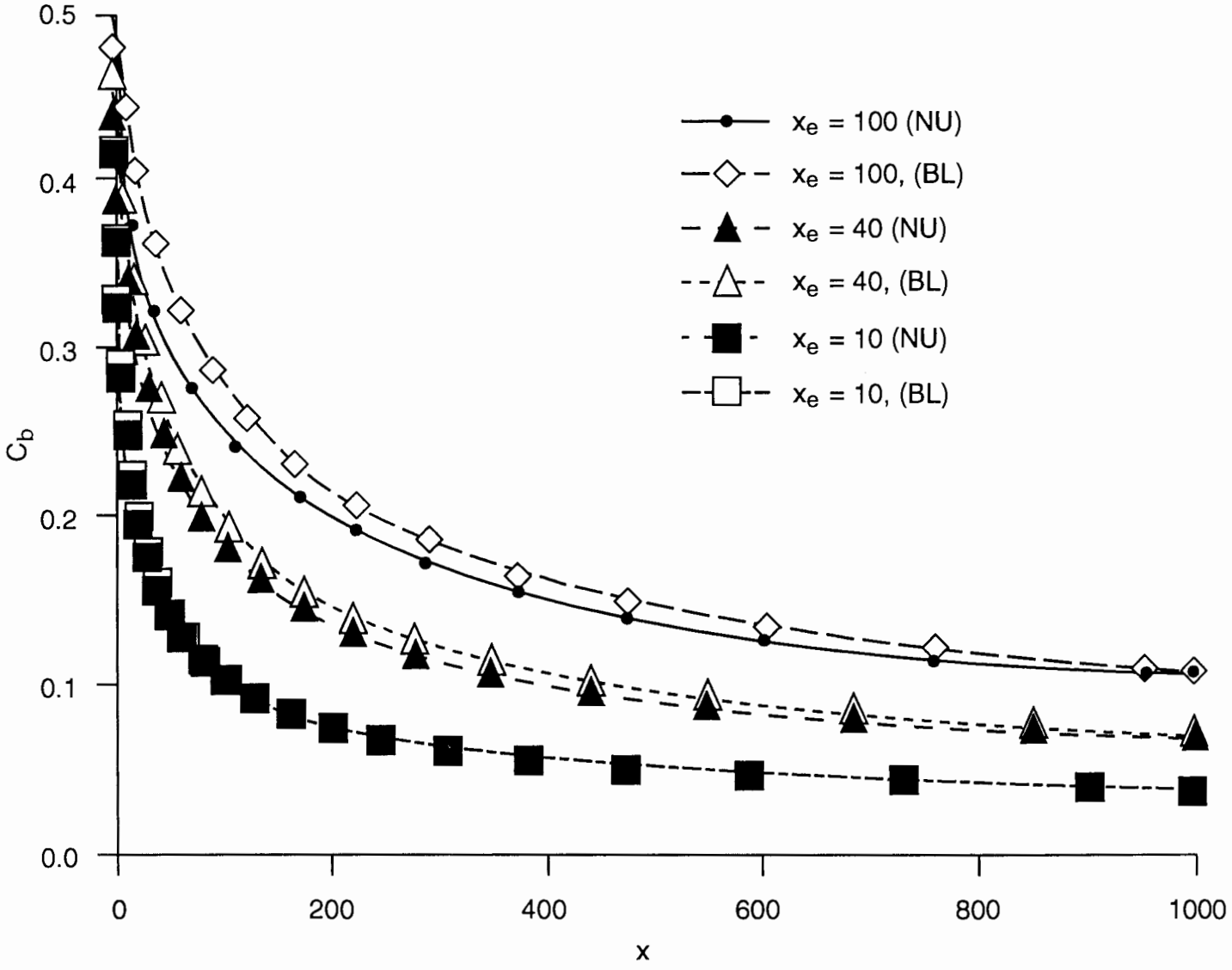

Fig. 10. Comparison of steady state profiles of C_b for various x_e-values ($a = 0.1$)

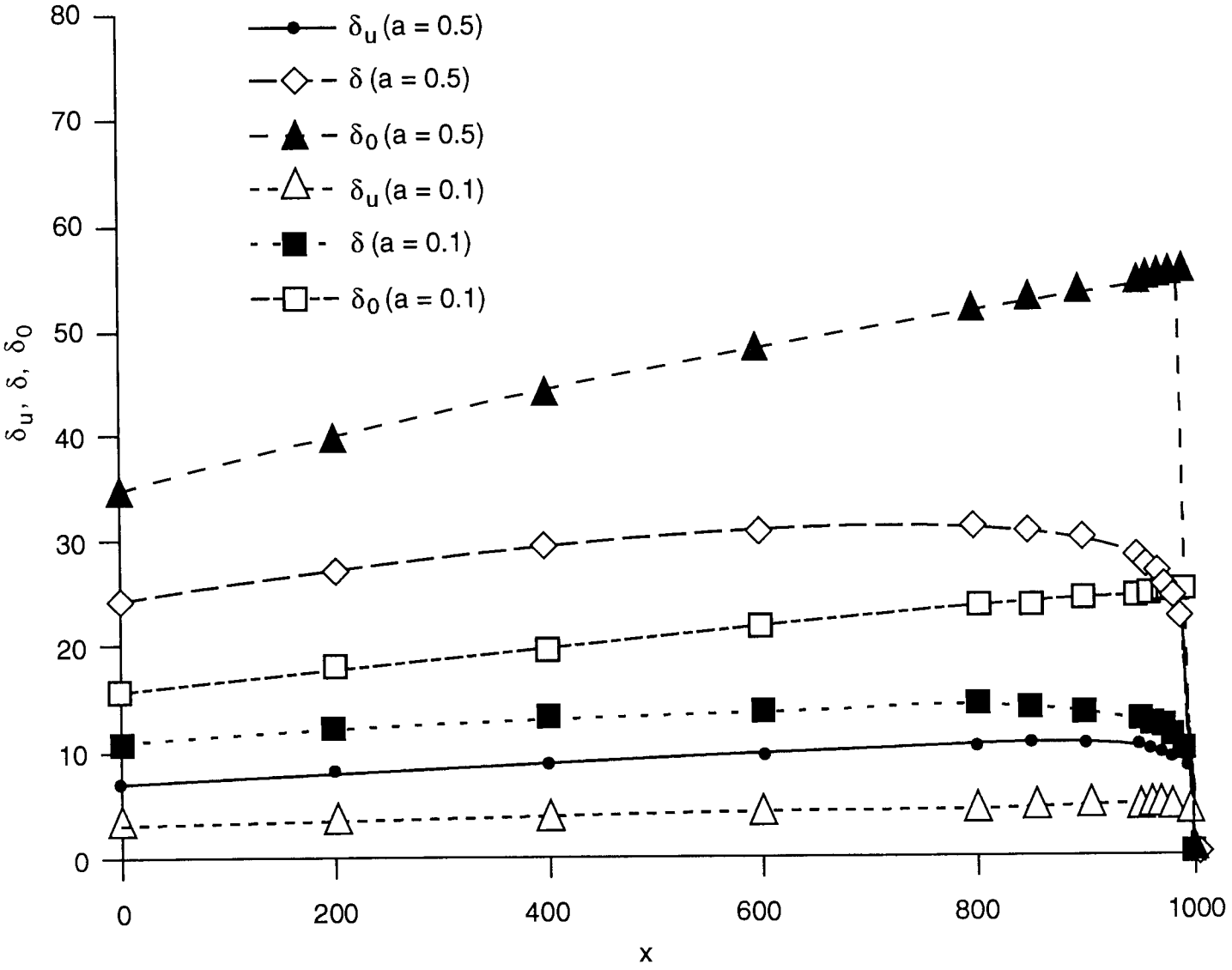

Fig. 11a Shapes of the BLs various -values ($a = 0.1, 0.5, x_e = 100$)

(a) $t = 100$

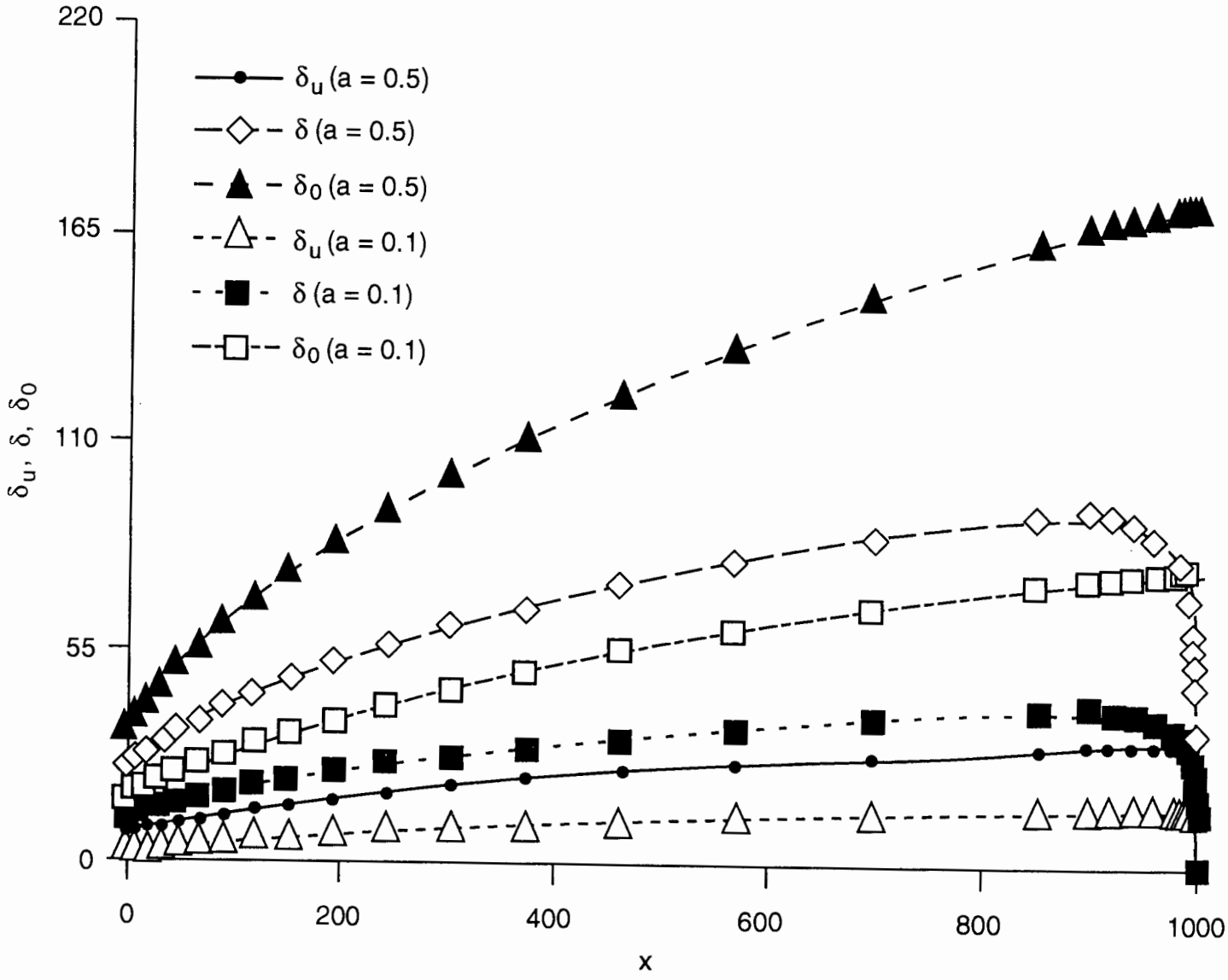

Fig. 11b Shapes of the BLs various -values (a = 0.1, 0.5, x_e = 100)

(b) t = 1000

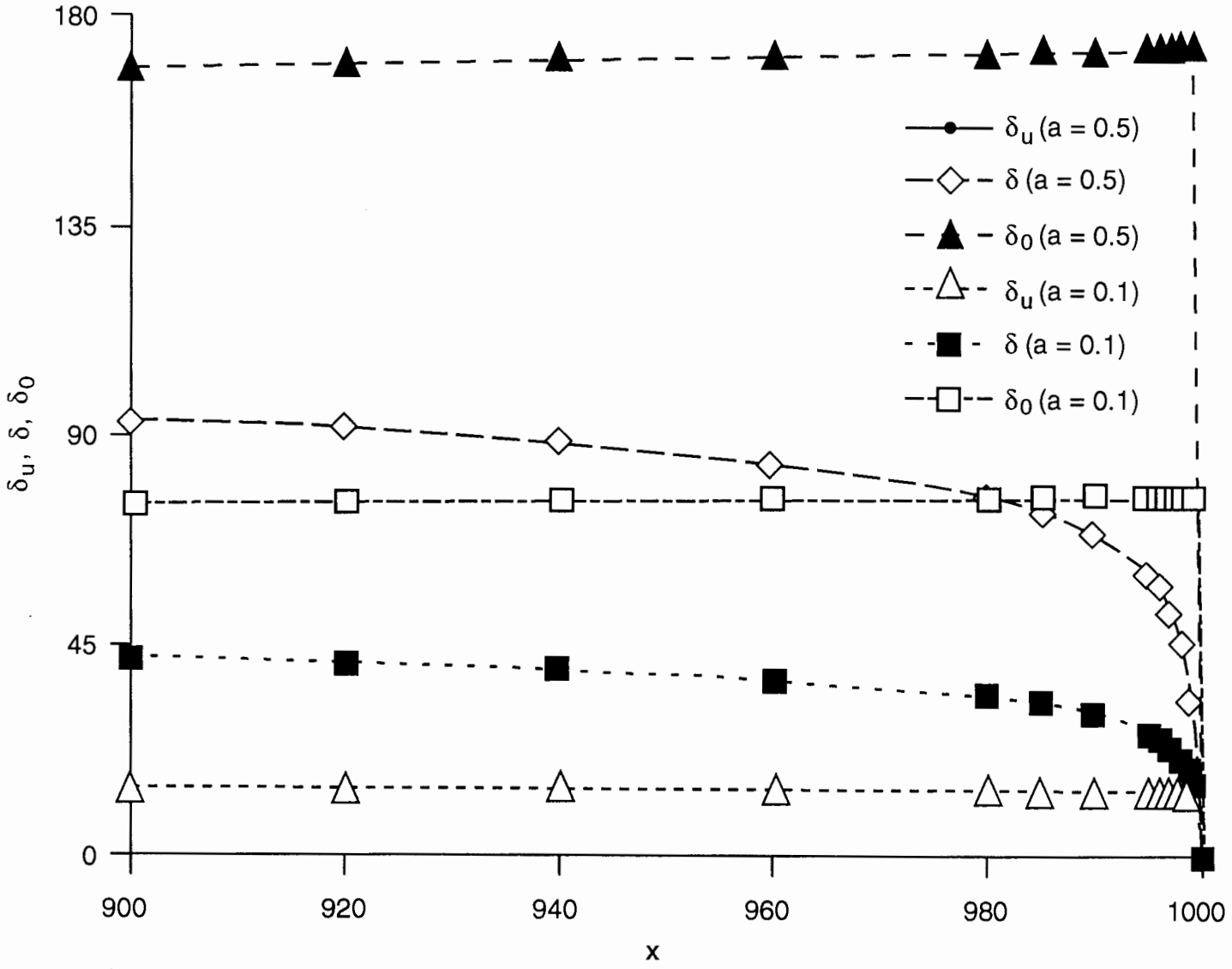

Fig. 11c Shapes of the BLs various -values ($a = 0.1, 0.5, x_e = 100$)

(c) $t = 1000$; spear-head region only

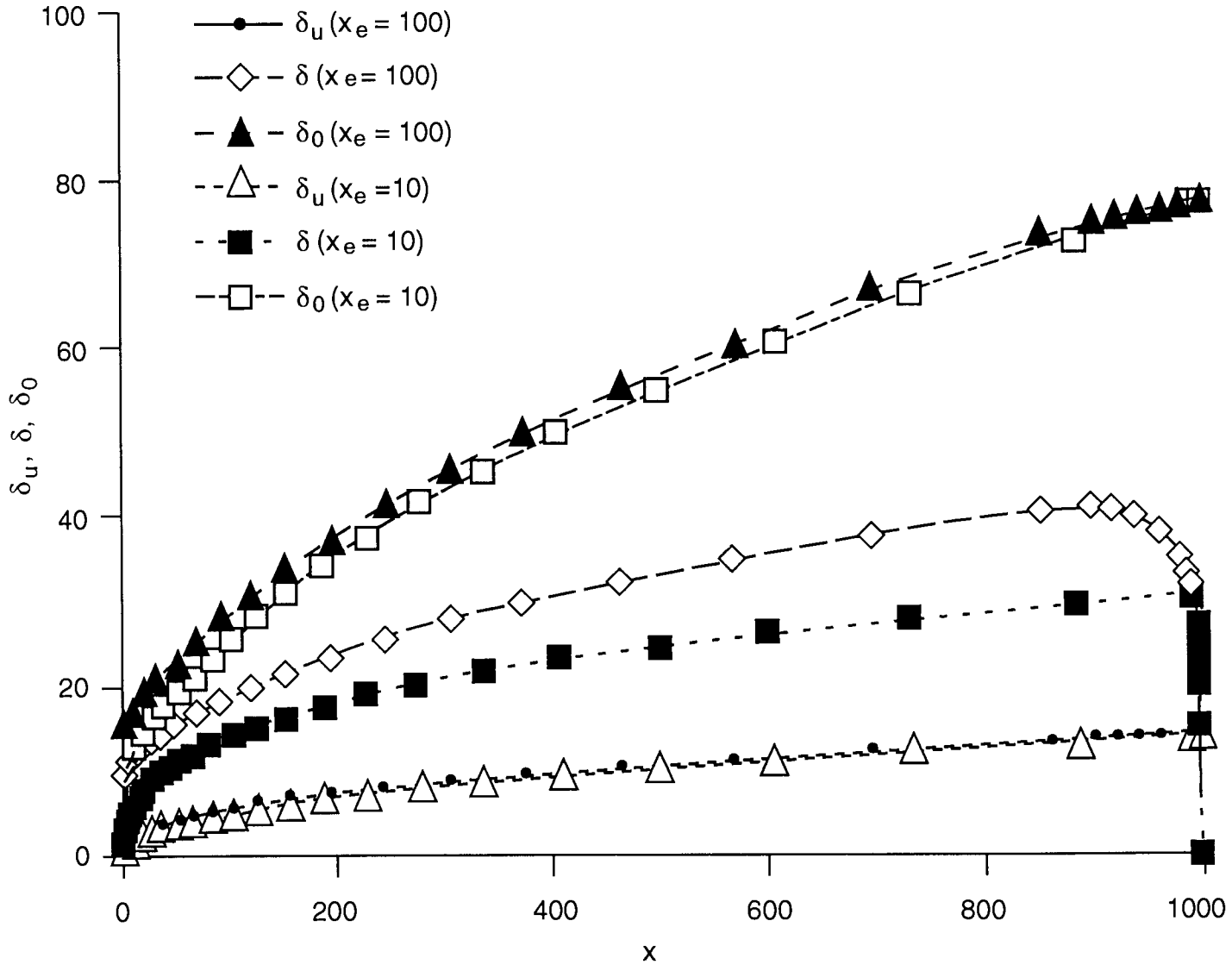

Fig. 12 Shapes of the BLs at $t = 1000$ for various x_e-values ($a = 0.1$)

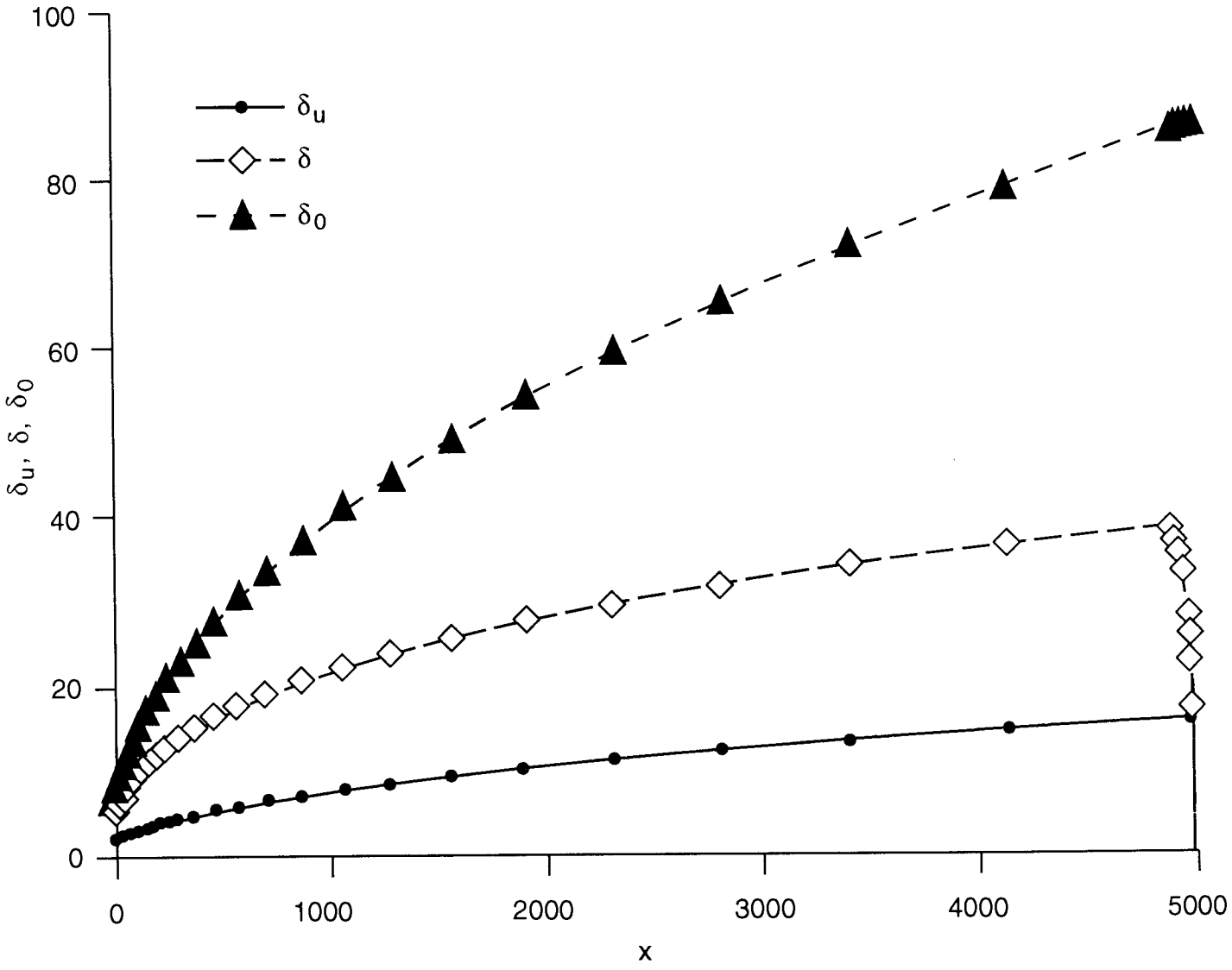

Fig. 13a Shapes of the BLs at $t = 5000$ ($a = 0.1$, $x_e = 100$)

(a) the complete domain

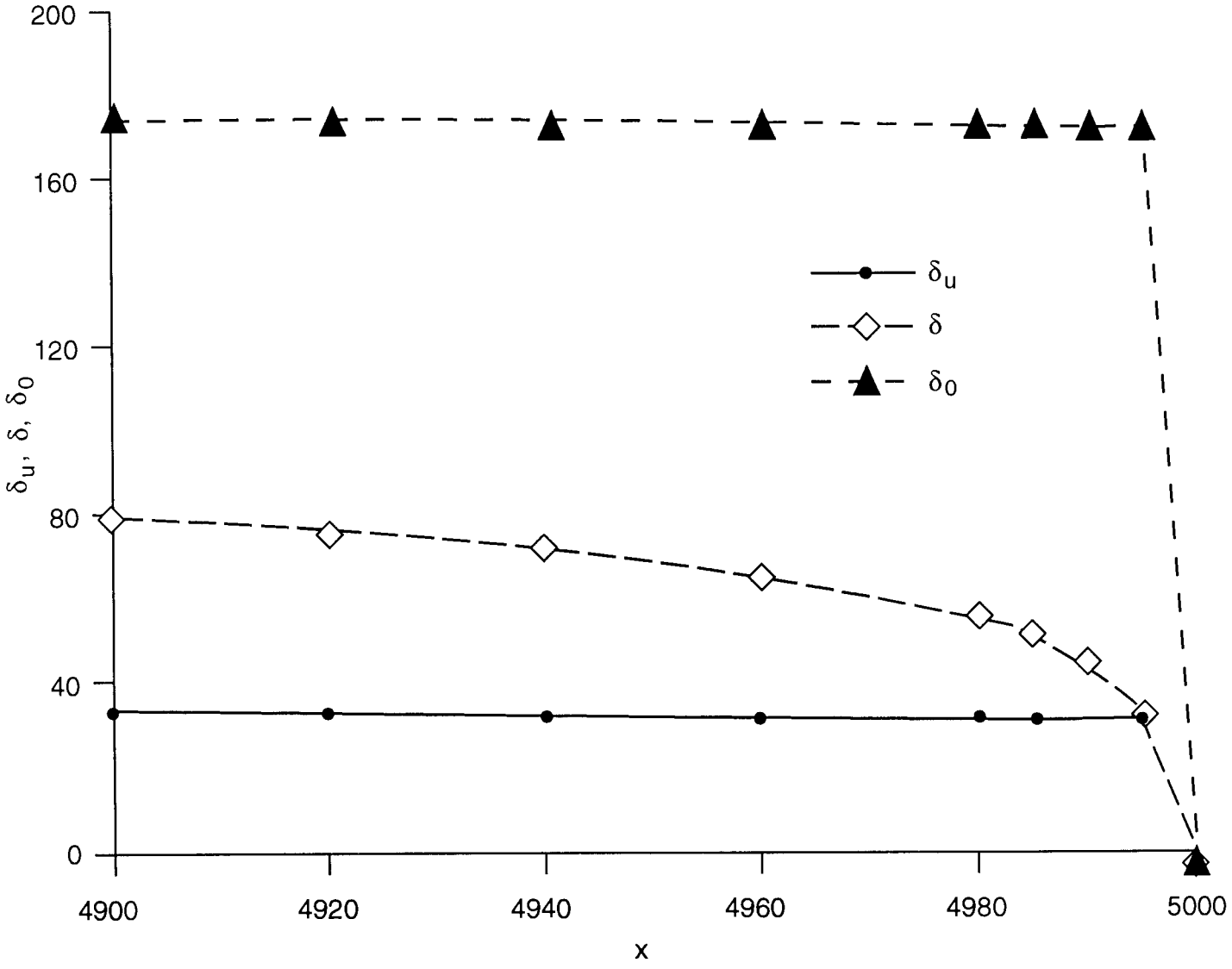

Fig. 13b Shapes of the BLs at $t = 5000$ ($a = 0.1$, $x_e = 100$)

(b) the spear-head region

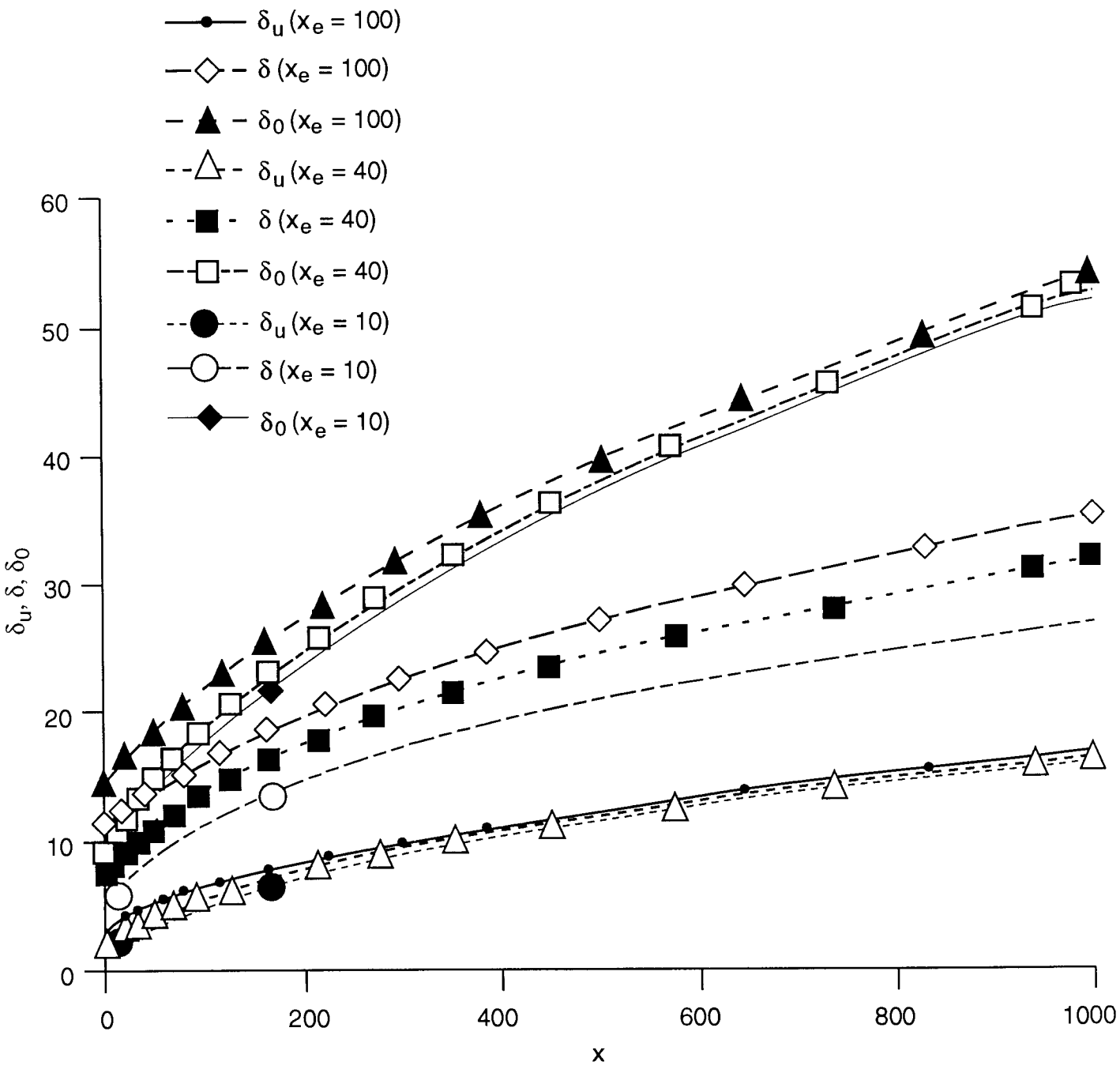

Fig. 14a Shapes of the BLs in the steady state region for various x_e-values

(a) $a = 0.1$

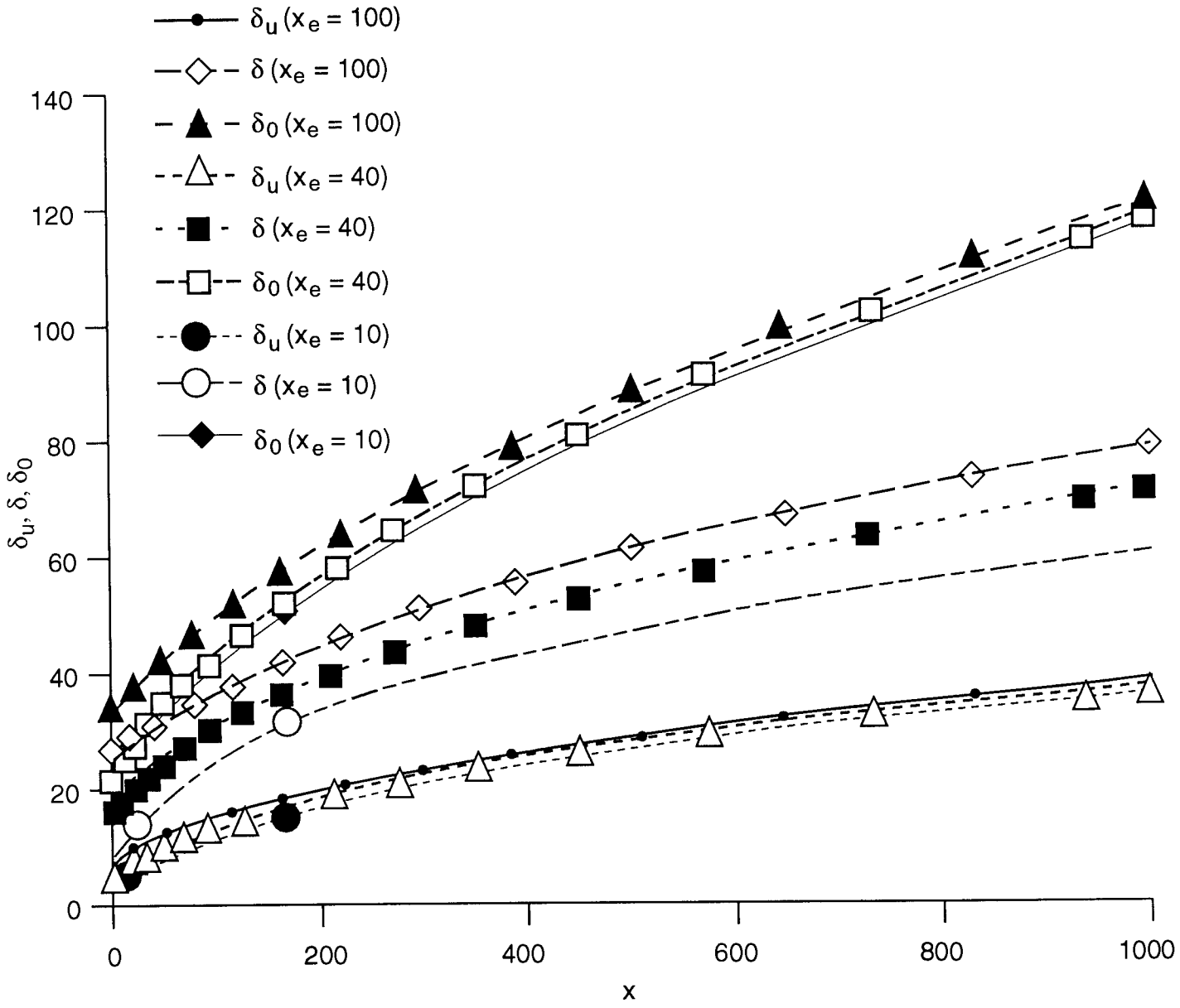

Fig. 14b Shapes of the BLs in the steady state region for various x_e-values

(b) $a = 0.5$

the decrease of δ with the increase of x-values was limited to the spearhead region. Values of δ_u and δ_0 in the spearhead region remained almost constant at large distances from the discontinuity.

Figure 14 demonstrates the effects of the discontinuity exposure length, x_e, and the dispersivity, a, on the development of the various BLs in the steady state region. As indicated by eq. (12) the effect of x_e was identical to that of the dispersivity, a, with regard to the build-up of the left-hand side boundary, at $x = 0$, of the domain $x, y \geq 0$. However, eqs. (30) and (37) indicate that the rate of expansion of δ_u and δ_0 with increasing x-values depended solely on the dispersivity, a. Fig. 14 exemplifies this phenomenon.

We might expect a comparatively large effect of longitudinal dispersion in the spearhead region, where longitudinal salinity gradients were not negligible. Therefore, we have performed a series of comparative simulations aimed at the evaluation of such an effect. We have simulated the salinity penetration at consecutive time intervals by employing the BL simulation approach as well as finite difference explicit schemes of eq. (6). The numerical scheme used was represented a combination of the explicit-implicit approach for first order hyperbolic equations (e.g. Lapidus and Pinder, 1982) and the explicit approach for the solution of parabolic differential equations. The numerical scheme obtained by such an arrangement was:

$$C_{r,s}^{m+1}\left(1+\frac{\Delta t}{\Delta x}\right)=C_{r,s}^{m}+C_{r-1,s}^{m+1}\frac{\Delta t}{\Delta x}+a\frac{\Delta t}{(\Delta y)^2}\left(C_{r,s+1}^{m}-2C_{r,s}^{m}+C_{r,s-1}^{m}\right)$$
$$+a_L\frac{\Delta t}{(\Delta x)^2}\left(C_{r+1,s}^{m}-2C_{r,s}^{m}+C_{r-1,s}^{m}\right) \qquad (53)$$

where m is the number of the time step.

Equation (53) is associated with the finite difference presentation of the boundary and initial conditions given by eqs. (13)–(18). Von Neumann's stability analysis of the numerical scheme given by eq. (53), indicated that this scheme was stable provided that the following criteria were satisfied (Rubin, 1994):

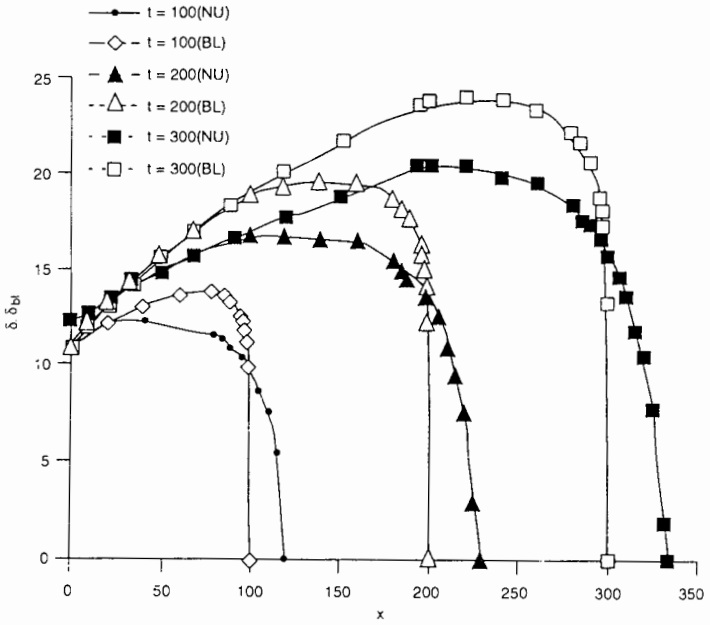

Figure 15(a)

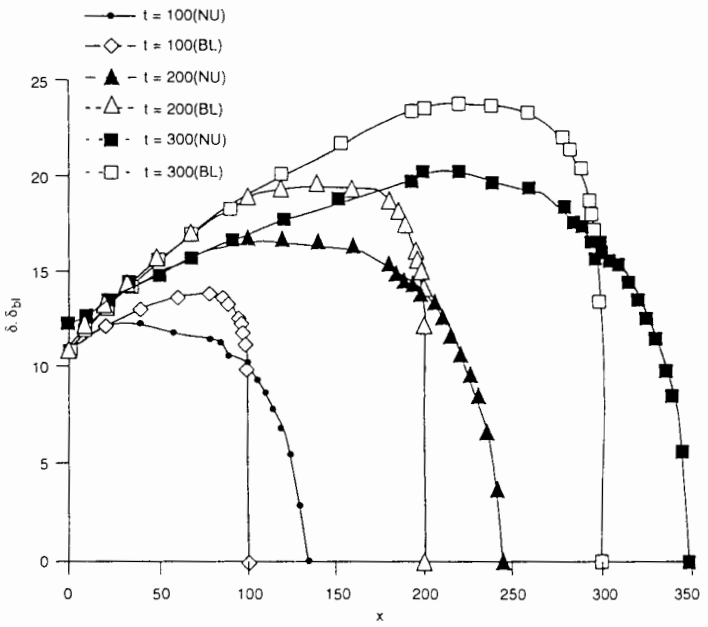

Figure 15(b)

Fig. 15. Comparisons between the salinity penetration according to the boundary layer (BL subscript) and numerical simulations

(a) comparison when longitudinal dispersion is neglected

(b) comparison while considering longitudinal dispersion

$$\frac{2a_L\Delta t}{(\Delta x)^2}+\frac{2a\Delta t}{(\Delta y)^2}\le 1+\frac{\Delta t}{\Delta x}$$
$$\frac{2a\Delta t}{(\Delta y)^2}\le 1 \qquad (54)$$

We have also performed simulations with the short version of eq. (53), in which the last term of this expression was neglected, namely neglecting the effect of the longitudinal dispersion on transport and distribution of salt in the simulated domain. In this short version only the last stability criterion of eq. (54) should be applied.

Results of both types of simulations were compared with results obtained by the use of the BL approach in Fig. 15. There were some differences between the BL simulations and results obtained by the employment of the numerical schemes. However, numerical results of the complete and short versions were very similar. Therefore, it seemed that differences between the BL and the numerical results were very much affected by numerical dispersion. Generally, the BL approach and the numerical simulations represented almost identical phenomena of salinity penetration into the freshwater aquifer. All approaches indicated that the region of interest (ROI), namely $0 \le y \le \delta$, increases with increasing x-values in the steady state region, even for very large values of x, and it decreased with increasing x-values in the spear-head region. The dimensionless horizontal extent of the salinity penetration was identical to the dimensionless time period of advection of the mineralized fluid particles.

Some practical applications

The method developed in this study has already been applied to the estimate of some phenomena associated with aquifer mineralization in Kansas. Garneau (1995) analyzed measurements of salinity in sets of boreholes drilled in Groundwater Management District 5 (GMD5), and followed the development of salinity profiles in various east-west cross sections of the aquifer. In

his study he applied the methods developed in the previous studies (Rubin and Buddemeier, 1998a, b) as well as the method of the present study. He could analyze salinity profiles in locations of direct contact between the saline and freshwater as well as profiles measured downstream of such locations. By comparing the field measurements with the TSBL method, presented in previous and present papers, he found values of the characteristic transverse dispersivities of the aquifer. He could also estimate the location of discontinuities of the impermeable layer. Furthermore, he could provide an estimate of the size of such discontinuities.

Young and Rubin (1998) have calculated possible infiltration of saline water from the deep bedrock into the freshwater aquifer, in locations of salinity penetration into the freshwater aquifer. They made measurements of salinity profiles in bundles of close monitoring wells penetrating to various shallow depths, and into the deep bedrock saline aquifer. They measured the pressure in all wells at particular locations, and made an integration of the density profile, to calculate the "effective hydrostatic pressure" in the bedrock aquifer. According to the difference between the measured pressure in the bedrock aquifer and its effective hydrostatic pressure, Young and Rubin (1998) calculated the rate of seepage of salt water from the bedrock aquifer to the freshwater zone. In some cases they found no seepage of saline water. In such cases salinity was transferred into the freshwater zone, through the discontinuity of the impermeable layers, by direct contact between the saline and fresh groundwater. The present part of the study refers to such a case. Part 2 of this study refers to cases of seepage of saline water into the fresh water zone through semipermeable discontinuities in the impermeable layer.

Quinodoz and Buddemeier (1997) divided GMD5 into three parallel strips extended from west to east. Each strip was divided into several sections. For each section of the aquifer strip, they calculated budgets of groundwater and salinity and estimated the amount of salt transported from the deep bedrock aquifer into the freshwater zone. They found that the total salt quantity transferred from the deep bedrock into freshwater bearing layers of GMD5 was about 120,000 ton/year (of Cl.). Most of this quantity was supplied through the northern strip of the region.

Their calculations could be used to verify the validity of some of the estimates of Garneau (1995).

Summary and Conclusions

Recent field measurements in south central Kansas, as well as some quantitative calculations, have indicated that phenomena of groundwater mineralization probably originate from local discontinuities in the clay layers and other types of impermeable layers. In comparison to this phenomenon, it should be noted that in much of the western part of Kansas, thick impermeable layers completely separate the freshwater aquifer from the deep Permian formation, which is saturated with saline water.

Previous studies of the authors (Rubin and Buddemeier, 1996; 1998a; b) concerned the development and possible use of the top specified boundary layer (TSBL) approach for the simulation of contaminant hydrology issues. Special interest has been given to cases of groundwater mineralization due to direct contact between fresh and saltwater, as well as due to seepage of saltwater into the freshwater aquifer.

Traditional or classical uses of the BL approach consider that the region of interest (ROI), in which the value of the transported quantity varies from significant to negligible, behaves as a BL. In that region BL laws of similarity are applicable. Due to this requirement of identity between the ROI and the region in which BL laws of similarity take place, the traditional BL approach can only be applied to Dirichlet type problems, namely cases in which the quantity value is specified at the boundary of the domain. By separating the definition of the ROI from the region in which BL similarity laws apply, the TSBL approach can be applied to various types of Dirichlet and Neumann problems, as well as combinations of such boundary conditions. However, in any particular case of study the appropriate definition of the ROI should be given, and regions of BL similarity should be identified. Furthermore, laws of similarity in such regions should be identified, and appropriate formulations for each similarity region should be adopted. We define the thickness of the ROI as δ. The thickness δ is measured in the direction perpendicular to the flow direction and the streamlines.

The present study concerned the penetration of salinity into the freshwater aquifer due to a discontinuity in the impermeable layer, which led to direct contact between the fresh and saltwater. The direct contact between the fresh and saltwater caused horizontal penetration of the salinity into freshwater regions, in which the local impermeable layer completely separated the freshwater aquifer from the deep bedrock saturated by saltwater. Simulation of this salinity penetration was achieved by dividing the vertical salinity profile into two BLs: (a) the inner BL - located close to the impermeable bottom of the aquifer, and (b) the outer BL - built on top of the inner BL.

The calculations indicated that the salinity horizontal penetration could be represented as a build-up of the ROI whose thickness was δ, and its longitudinal extent was identical to the advection length of the mineralized fluid particles. It was possible to identify two regions in the horizontal extent of the salinity penetration: (a) the steady state region, and (b) the spearhead region. In the steady state region the thickness of the ROI increased moderately with increasing x-values. The horizontal extent of the spearhead region was identical to that of the discontinuity that exposes the freshwater to direct contact with saltwater. In the evaluated example of this report, even at large distances from the discontinuity exposure, any decrease of the ROI thickness with increasing values of x was found to be limited to the spearhead region. At the downstream end of the spearhead region the thickness of the ROI vanished.

Comparative simulations with the BL method as well as with various types of finite difference numerical schemes have indicated the adequacy of the TSBL approach for the simulation of the salinity penetration into regions of complete separation at the fresh- and salt-water aquifers by impermeable layers between them.

The method developed in this study has been applied to practical issues concerning mineralization of groundwater in south central Kansas.

ACKNOWLEDGMENTS

This work was supported under contracts between the Kansas Water Office and the Kansas Geological Survey. The authors are grateful for the assistance of Mark Schoneweis in preparing the illustrations.

Notation

a dimensionless transverse dispersivity

aL dimensionless longitudinal dispersivity

BL boundary layer

c_r ratio between C and C_b at the boundary between the inner and outer boundary layers

C dimensionless salinity

C_b dimensionless salinity at the bottom of the aquifer

C_T dimensionless salinity at the top of the ROI

C_{avo} dimensionless average salinity at the outer boundary layer

C_{avu} dimensionless average salinity at the inner boundary layer

C^* salt concentration – salinity [ML^{-3}]

C_f^* salinity of the freshwater aquifer [ML^{-3}]

C_s^* salinity of the saltwater [ML^{-3}]

$\tilde{D}$ dispersion tensor [L^2T^{-1}]

D_x longitudinal dispersion coefficient [L^2T^{-1}]

D_y transverse dispersion coefficient [L^2T^{-1}]

g gravitational acceleration [LT^{-2}]

k permeability [L^2]

l_0 length scale[L]

m number of the time step

n power coefficient of boundary layer series expansion at $-x_e = x = 0$

n_1 power coefficient of inner boundary layer

n_2 power coefficient of outer boundary layer

NU numerical simulation value

p pressure [$ML^{-1}T^{-2}$]

q specific discharge [LT^{-1}]

r number of nodal point in the x-direction

ROI region of interest

s number of nodal point in the y-direction

t dimensionless time

t_0 dimensionless time at which the mineralized fluid particle is at $x = 0$

t^* time (T)

TSBL top specified boundary layer

TZ transition zone

u unit step function

V interstitial flow velocity [LT^{-1}]

x dimensionless longitudinal coordinate

x_e dimensionless extent of the impermeable layer discontinuity

x_{max} dimensionless extent of the simulated domain

x^* longitudinal coordinate [L]

x_e^* length of the discontinuity [L]

y dimensionless vertical coordinate

y^* vertical coordinate [L]

α_1 coefficient defined in eq. (25)

α_2 coefficient defined in eq. (33)

δ dimensionless thickness of the ROI

δ_u dimensionless thickness of the inner boundary layer

δ_0 dimensionless thickness of the combined inner and outer boundary layers

δ_R ratio between δ_0 and δ_u

Δt time step

Δx longitudinal interval

Δy vertical interval

η outer boundary layer coordinate

η_T value of η at $y = \delta$ (provided that $\delta_u < \delta < \delta_0$)

μ viscosity [$ML^{-1}T^{-1}$]

ξ inner boundary layer coordinate

ξ_T value of ξ at $y = \delta$ (provided that $0 < \delta < \delta_u$)

ρ fluid density [ML^{-3}]

References

Buddemeier, R.W., Sophocleous, M.A. and Whittemore, D.O., 1992. Mineral intrusion—Investigation of salt contamination of groundwater in the Eastern Great Bend Prairie Aquifer, Open-File Report 92-25, Geohydrology, Kansas Geological Survey, The University of Kansas, Lawrence, KS.

Buddemeier, R.W., Garneau, G.W., Young, D.P., Whittemore, D.O., Zehr, D., Lanterman, J., Ma, T.S., and Falk, S., 1994. The mineral intrusion project: Progress and activities during fiscal year 1994, Open-File Report 94-28, Geohydrology, Kansas Geological Survey, The University of Kansas, Lawrence, KS.

Carslaw, H.S. and Jaeger, J.C., 1959. Conduction of Heat in Solids. Oxford at the Clarendon Press, London.

Cobb, P.M., 1980. The distribution and mechanisms of salt water intrusion in the fresh water aquifer and in Rattlesnake Creek Stafford County Kansas, M.S. thesis, Department of Civil Engineering, The University of Kansas, Lawrence, KS.

Fader, S.W. and Stullken, L.E., 1978. Geohydrology of the Great Bend Prairie South-Central Kansas, Irrigation Series 4, Kansas Geological Survey.

Fischer, H.B., List, E., Koh, R.C.Y., Imberger, J. and Brooks, N.H., 1979. Mixing in Inland and Coastal Waters, Academic Press, NY.

Garneau, G.W., 1995. Detection and Characterization of the distribution of mineral intrusion in the Great Bend Prairie Aquifer – south-central Kansas, Kansas Geological Survey Open-File Report 95-35, Lawrence, KS.

Hill, J.M. and Dewynne, J.N., 1987. Heat Conduction, Blackwell, Oxford, U.K.

Lapidus, L. and Pinder, G.F., 1982. "Numerical solution of Partial Differential Equations in Science and Engineering, " John-Wiley & Sons, NY.

Latta, B., 1950. Geology and groundwater resources of Barton and Stafford Counties, Kansas Bulletin 88, Kansas Geological Survey.

Layton, D.W. and Berry, D.W., 1973. Geology and Ground-water resources of Pratt County, South-Central Kansas, Bulletin 205, Kansas Geological Survey.

Garneau, G.W., 1995. Detection and Characterization of the distribution of mineral intrusion in the Great Bend Prairie Aquifer – south-central Kansas, Kansas Geological Survey Open-File Report 95-35, Lawrence, KS.

Rubin, H., 1994. Numerical schemes applicable in contaminant hydrology, Open-File Report 94-8, Geohydrology, Kansas Geological Survey, The University of Kansas, Lawrence, KS.

Rubin, H. and Buddemeier, R.W., 1996. A top specified boundary layer (TSBL) approximation approach for the simulation of groundwater contamination processes, Journal of Contaminant Hydrology, 22: 123 – 144.

Rubin, H. and Buddemeier, R.W., 1998a. Application of the top specified boundary layer (TSBL) approximation to initial characterization of an inland aquifer mineralization, Part 1: Direct contact between fresh and saltwater, Journal of Contaminant Hydrology, 32/3-4: 149-172.

Rubin, H. and Buddemeier, R.W., 1998b. Application of the top specified boundary layer (TSBL) approximation to initial characterization of an inland aquifer mineralization, Part 2: Seepage of saltwater, Journal of Contaminant Hydrology, 32/3-4: 173-198.

Whittemore, D.O., 1993. Ground water geochemistry in the mineral intrusion area of groundwater management district no. 5, South-Central Kansas, Kansas Geological Survey, The University of Kansas, Lawrence, KS.

Young, D.P., 1992. Mineral intrusion: Geohydrology of Permian bedrock underlying the Great Bend Prairie aquifer in south-central Kansas, Open-File Report 92-44, Geohydrology, Kansas Geological Survey, The University of Kansas, Lawrence, KS.

Young, D. and Rubin, H., 1998. Determining vertical flow in variable density groundwater - a hydrostatic approach applied in south-central Kansas, Eighteenth Annual Hydrology Days, Colorado State University, Fort Collins, Colorado, March 30-April 3, 1998